

World Journal of *Radiology*

World J Radiol 2018 October 28; 10(10): 116-142





EDITORIAL

- 116 Could intravoxel incoherent motion diffusion-weighted magnetic resonance imaging be feasible and beneficial to the evaluation of gastrointestinal tumors histopathology and the therapeutic response?
Zuo HD, Zhang XM

ORIGINAL ARTICLE

Observational Study

- 124 Reproducibility of thrombus volume quantification in multicenter computed tomography pulmonary angiography studies
Kaufman AE, Pruzan AN, Hsu C, Ramachandran S, Jacobi A, Patel I, Schwacho L, Mercuri MF, Fayad ZA, Mani V
- 135 Low-radiation and high image quality coronary computed tomography angiography in "real-world" unselected patients
Richards CE, Dorman S, John P, Davies A, Evans S, Ninan T, Martin D, Kannoly S, Roberts-Davies G, Ramsey M, Obaid DR

ABOUT COVER

Editorial Board Member of *World Journal of Radiology*, Xin-Wu Cui, PhD, Professor, Department of Medical Ultrasound, Tongji Hospital of Tongji Medical College, Huazhong University of Science and Technology, Wuhan 430030, Hubei Province, China

AIM AND SCOPE

World Journal of Radiology (*World J Radiol*, *WJR*, online ISSN 1949-8470, DOI: 10.4329) is a peer-reviewed open access academic journal that aims to guide clinical practice and improve diagnostic and therapeutic skills of clinicians.

WJR covers topics concerning diagnostic radiology, radiation oncology, radiologic physics, neuroradiology, nuclear radiology, pediatric radiology, vascular/interventional radiology, medical imaging achieved by various modalities and related methods analysis. The current columns of *WJR* include editorial, frontier, diagnostic advances, therapeutics advances, field of vision, mini-reviews, review, topic highlight, medical ethics, original articles, case report, clinical case conference (clinicopathological conference), and autobiography.

We encourage authors to submit their manuscripts to *WJR*. We will give priority to manuscripts that are supported by major national and international foundations and those that are of great basic and clinical significance.

INDEXING/ABSTRACTING

World Journal of Radiology is now abstracted and indexed in Emerging Sources Citation Index (Web of Science), PubMed, PubMed Central, China National Knowledge Infrastructure (CNKI), and Superstar Journals Database.

EDITORS FOR THIS ISSUE

Responsible Assistant Editor: *Xiang Li*
Responsible Electronic Editor: *Yun-XiaoJian Wu*
Proofing Editor-in-Chief: *Lian-Sheng Ma*

Responsible Science Editor: *Fang-Fang Ji*
Proofing Editorial Office Director: *Jin-Lei Wang*

NAME OF JOURNAL
World Journal of Radiology

ISSN
 ISSN 1949-8470 (online)

LAUNCH DATE
 January 31, 2009

FREQUENCY
 Monthly

EDITORS-IN-CHIEF
Kai U Juergens, MD, Associate Professor, MRT und PET/CT, Nuklearmedizin Bremen Mitte, ZEMODI - Zentrum für morphologische und molekulare Diagnostik, Bremen 28177, Germany

Edwin JR van Beek, MD, PhD, Professor, Clinical Research Imaging Centre and Department of Medical Radiology, University of Edinburgh, Edinburgh EH16 4TJ, United Kingdom

Thomas J Vogl, MD, Professor, Reader in Health Technology Assessment, Department of Diagnostic and Interventional Radiology, Johann Wolfgang Goethe University of Frankfurt, Frankfurt 60590,

Germany

EDITORIAL BOARD MEMBERS
 All editorial board members resources online at <http://www.wjnet.com/1949-8470/editorialboard.htm>

EDITORIAL OFFICE
 Jin-Lei Wang, Director
World Journal of Radiology
 Baishideng Publishing Group Inc
 7901 Stoneridge Drive, Suite 501, Pleasanton, CA 94588, USA
 Telephone: +1-925-2238242
 Fax: +1-925-2238243
 E-mail: editorialoffice@wjnet.com
 Help Desk: <http://www.f6publishing.com/helpdesk>
<http://www.wjnet.com>

PUBLISHER
 Baishideng Publishing Group Inc
 7901 Stoneridge Drive, Suite 501, Pleasanton, CA 94588, USA
 Telephone: +1-925-2238242
 Fax: +1-925-2238243
 E-mail: bpgoffice@wjnet.com
 Help Desk: <http://www.f6publishing.com/helpdesk>
<http://www.wjnet.com>

PUBLICATION DATE
 October 28, 2018

COPYRIGHT
 © 2018 Baishideng Publishing Group Inc. Articles published by this Open-Access journal are distributed under the terms of the Creative Commons Attribution Non-commercial License, which permits use, distribution, and reproduction in any medium, provided the original work is properly cited, the use is non commercial and is otherwise in compliance with the license.

SPECIAL STATEMENT
 All articles published in journals owned by the Baishideng Publishing Group (BPG) represent the views and opinions of their authors, and not the views, opinions or policies of the BPG, except where otherwise explicitly indicated.

INSTRUCTIONS TO AUTHORS
<http://www.wjnet.com/bpg/gerinfo/204>

ONLINE SUBMISSION
<http://www.f6publishing.com>

Could intravoxel incoherent motion diffusion-weighted magnetic resonance imaging be feasible and beneficial to the evaluation of gastrointestinal tumors histopathology and the therapeutic response?

Hou-Dong Zuo, Xiao-Ming Zhang

Hou-Dong Zuo, Xiao-Ming Zhang, Sichuan Key Laboratory of Medical Imaging, Department of Radiology, Affiliated Hospital of North Sichuan Medical College, Nanchong 637000, Sichuan Province, China

ORCID number: Hou-Dong Zuo (0000-0002-1530-3018); Xiao-Ming Zhang (0000-0001-5327-8506).

Author contributions: All authors contributed to writing the paper and had full control over preparation of manuscript; all authors approved the final draft manuscript.

Conflict-of-interest statement: None.

Open-Access: This article is an open-access article which was selected by an in-house editor and fully peer-reviewed by external reviewers. It is distributed in accordance with the Creative Commons Attribution Non Commercial (CC BY-NC 4.0) license, which permits others to distribute, remix, adapt, build upon this work non-commercially, and license their derivative works on different terms, provided the original work is properly cited and the use is non-commercial. See: <http://creativecommons.org/licenses/by-nc/4.0/>

Manuscript source: Invited manuscript

Correspondence to: Xiao-Ming Zhang, MD, PhD, Professor, Sichuan Key Laboratory of Medical Imaging, Department of Radiology, Affiliated Hospital of North Sichuan Medical College, 63# Wenhua Road, Shunqing District, Nanchong 637000, Sichuan Province, China. cjr.zhxm@vip.163.com
Telephone: +86-817-2262218
Fax: +86-817-2222856

Received: June 23, 2018

Peer-review started: June 24, 2018

First decision: July 19, 2018

Revised: August 2, 2018

Accepted: August 2, 2018

Article in press: August 26, 2018

Published online: October 28, 2018

Abstract

Gastrointestinal tumors (GTs) are among the most common tumors of the digestive system and are among the leading causes of cancer death worldwide. Functional magnetic resonance imaging (MRI) is crucial for assessment of histopathological changes and therapeutic responses of GTs before and after chemotherapy and radiotherapy. A new functional MRI technique, intravoxel incoherent motion (IVIM), could reveal more detailed useful information regarding many diseases. Currently, IVIM is widely used for various tumors because the derived parameters (diffusion coefficient, D ; pseudo-perfusion diffusion coefficient, D^* ; and perfusion fraction, f) are thought to be important surrogate imaging biomarkers for gaining insights into tissue physiology. They can simultaneously reflect the microenvironment, microcirculation in the capillary network (perfusion) and diffusion in tumor tissues without contrast agent intravenous administration. The sensitivity and specificity of these parameters used in the evaluation of GTs vary, the results of IVIM in GTs are discrepant and the variability of IVIM measurements in response to chemotherapy and/or radiotherapy in these studies remains a source of controversy. Therefore, there are questions as to whether IVIM diffusion-weighted MRI is feasible and helpful in the evaluation of GTs, and whether it is worthy of expanded use.

Key words: Intravoxel incoherent motion; Metastasis; Gastric cancer; Colorectal cancer

© **The Author(s) 2018.** Published by Baishideng Publishing Group Inc. All rights reserved.

Core tip: In general, the gastrointestinal tumors (GTs) can be diagnosed by routine computed tomography/magnetic resonance imaging (MRI) and biopsy, but the

intravoxel incoherent motion (IVIM), a new emerging MRI technique, plays an important role in the tumor evaluation before and after surgery, and provides more useful information in tumor properties, stage and chemoradiotherapy (CRT) response. What's more, the quantitative parameters derived from IVIM, including D, D* and f, can gain an insight into tumor tissue physiology changes and simultaneously reflect the microenvironment, microcirculation in the capillary network and diffusion in tumor tissues, thus, new imaging biomarkers for monitoring and evaluating the tumor and the CRT response in GTs.

Zuo HD, Zhang XM. Could intravoxel incoherent motion diffusion-weighted magnetic resonance imaging be feasible and beneficial to the evaluation of gastrointestinal tumors histopathology and the therapeutic response? *World J Radiol* 2018; 10(10): 116-123 Available from: URL: <http://www.wjgnet.com/1949-8470/full/v10/i10/116.htm> DOI: <http://dx.doi.org/10.4329/wjr.v10.i10.116>

INTRODUCTION

Gastrointestinal tumors (GTs) are common tumors of the digestive system and are among the leading causes of cancer death worldwide^[1]. It was estimated that there will be 176960 new cases and 62880 deaths in United States in 2018^[2]. The current therapeutic methods for GTs are surgical resection and chemotherapy and/or chemoradiotherapy (CRT)^[3]. However, surgery inflicts substantial trauma to both the body and mind. For advanced stage patients, systemic chemotherapy is the better choice. In this situation, imaging monitoring for the chemotherapeutic response and evaluation is essential. Magnetic resonance imaging (MRI) is a promising modality for tumor detection, diagnosis and evaluation, because of its many advantages, including absence of radiation, multiplane and multiple-parameter imaging. Diffusion weighted imaging (DWI) is an important imaging sequence, based on the Brownian motion of water molecules^[4]. The apparent diffusion coefficient (ADC) is sensitive to water molecules in the tissues and reflects the microenvironmental changes of tumors^[5]. It is used to differentiate malignant from benign tumors and to evaluate tumor responses after chemotherapy^[6,7]. However, ADC values of the tumor are not consistent after treatment because treatment may cause cell swelling or fibrosis that decreases ADC values^[8]. Based on the ADC reflection of the tissue diffusion and perfusion, Le Bihan *et al.*^[9] proposed the intravoxel incoherent motion (IVIM) model to depict perfusion and diffusion effects. It is a new dual exponential imaging mode with multiple b values that is applied in oncologic imaging and related studies^[10,11]. With multiple b values, IVIM-DWI quantifies microvascular perfusion effects with smaller b-values (0-200 s/mm²), and quantifies tissue water molecular diffusion with higher b-values (> 200 s/mm²). Therefore, IVIM-DWI MRI differentiates microvascular

perfusion activity from diffusion. Consequently, the following parameters derived from IVIM DW-MRI can be calculated without the contrast: (Slow) diffusion coefficient (D), pseudo-perfusion (fast) diffusion coefficient (D*) and perfusion fractions, (f)^[9,12]. The f and D* parameters have the potential to reflect tumor angiogenesis activity noninvasively and are significantly correlated with microvessel density (MVD) scores^[13]. D is generally thought to be the pure diffusion coefficient that depicts extracellular and extravascular tissue water molecular motion^[14]. Since IVIM-DWI was introduced, this technique showed great potential in tumor evaluation and grading^[15,16]. In recent years, IVIM-DWI has also been used to distinguish benign from malignant tumors^[17] and to evaluate chemotherapy therapeutic responses in various tumors^[10,18]. However, the application of IVIM-DWI in the gastrointestinal tract tumors may be challenged: first, gastrointestinal tract tumors are relatively small and thin, and imaging may be affected by motion artifact; second, the exact nature of the IVIM signal is not well-understood, and there are heterogeneous patterns of signal attenuation on a voxelwise basis in normal tissues and tumors^[19,20]; third, the sensitivity and specificity of these parameters used in the evaluation of GTs vary and the results of the IVIM in the GTs are discrepant^[15,18]; finally, the variability of IVIM measurements in response to chemotherapy and/or radiotherapy in these studies remains controversial^[10]. Nevertheless, the following findings in GTs may dispel our worries to some extent and may provide hope for the use of IVIM for GTs.

GASTRIC TUMORS

Few studies reported the IVIM-DWI was used in the gastric cancers, because gastric cancer can be diagnosed by contrast computed tomography (CT)/MRI^[21] and may be confirmed by endoscopy and biopsy^[22]. Nevertheless, IVIM has been used to evaluate the biological behavior of gastric cancer, including cell proliferation, differentiation, invasion, metastasis and survival^[23-25], as well as to monitor chemotherapeutic responses^[10,26]. D* and f values correlated with MVD in tumor tissues^[13], suggesting that D* and f might serve as imaging markers for the noninvasive evaluation of MVD of tumor grading and treatment effectiveness.

In fifty-three patients with gastric cancer reported by Ji *et al.*^[25], the D value positively correlated with human epidermal growth factor receptor-2 (HER2) scores ($r = 0.481$, $P < 0.001$), and the D values of HER2(+) gastric cancers were substantially higher than those of HER2(-) tumors ($P = 0.007$). With the cut-off value of $1.123 \times 10^{-3} \text{ mm}^2/\text{s}$, the D value differentiated HER2(+) from HER2(-) gastric cancers with an area under the curve of 0.762 ($P = 0.011$). Therefore, the IVIM-DWI is feasible for preoperative assessment of HER2 status of gastric cancers and could be a potential biomarker in evaluating HER2 status of gastric cancers.

As for chemotherapeutic responses, IVIM-DWI and derived parameters are useful for predicting the

early efficacy of chemotherapy and are more sensitive imaging biomarkers for gastric cancer. In mouse models bearing two kinds of human gastric cancer xenografts, and in human gastric adenocarcinoma AGS cells models (baseline: day 0), when the mouse received 5-fluorouracil (5-FU) (15 mg/kg)/calcium folinate (5 mg/kg) treatment, mean D values in the treated groups ($\Delta D\%$: 17.12% \pm 8.20%, 24.16% \pm 16.87%, 38.54% \pm 19.36%) were significantly higher than those of the controls ($\Delta D\%$: -0.13% \pm 4.23%, 5.89% \pm 4.56%, 5.54% \pm 4.44%) at days 1, 3, 5 and 7. The f values were significantly lower than those of the control group (-34.13% \pm 16.61% vs 1.68% \pm 3.40%; -50.64% \pm 6.82% vs 3.01% \pm 6.50%; -49.93% \pm 6.05% vs 0.97% \pm 4.38% and -46.22% \pm 7.75% vs 8.14% \pm 6.75%). The D* values were also significantly lower than those of the control group at all-time points (-32.10% \pm 12.22% vs 1.85% \pm 5.54%; -44.14% \pm 14.83% vs 2.29% \pm 10.38%; -59.06% \pm 19.10% vs 3.86% \pm 5.10% and -47.20% \pm 20.48% vs 7.13% \pm 9.88%). Furthermore, the histopathologic findings showed that D positively correlated with tumor necrosis and cellular apoptosis. Values of f and D* correlated positively with MVD and negatively correlated with cellular apoptosis^[26]. In MKN-45 human gastric adenocarcinoma xenograft mouse models, after fluorouracil and calcium folinate treatment, D* values in the treated group decreased markedly ($\Delta D^* = -30\%$, -34% and -20% , $P < 0.05$) and f values increased dramatically ($\Delta f = 93\%$, 113% and 181% , $P < 0.05$) on days 3, 7 and 14. D* and f values correlated well with histopathological changes demonstrating the reduction of cell proliferation and MVD and the increase in tumor apoptosis and necrosis^[10]. These findings indicated that IVIM-DWI and derived parameters could be potentially useful for early evaluation of chemotherapy response and may provide additional pivotal information for the evaluation of therapeutic effect in gastric tumors (Figure 1).

COLORECTAL TUMORS

Many studies focusing on the new techniques for the evaluation of the colorectal tumors have been published^[27,28]. A newly proposed modified VARIABLE PROjection (VARPRO) algorithm specifically tailored for fitting the IVIM to DWI showed better performance than did the Levenberg-Marquardt (LM) algorithm in 64% of cases and stronger "segmented" methods in 100% of cases in locally advanced rectal cancer (LARC). Therefore, VARPRO algorithm is a better fit for the IVIM model than is LARC DWI^[28].

In colorectal tumors, IVIM and the parameters were used to evaluate tumor histopathology, Kirsten rat sarcoma viral oncogene homologue (KRAS) mutation status, CRT response, pathological response to neoadjuvant chemotherapy (NACT) and relationships with tumor prognostic markers^[11,29-32].

IVIM-DWI has been explored in genomic expression experiments to predict the genotype of rectal cancer

(KRAS mutant/wild type)^[29]. D values were significantly lower and D* values were significantly higher in the KRAS mutant group than in the KRAS wild-type group. According to the ROC curve, D* values displayed moderate diagnostic significance with the area under curve (AUC) values of 0.710. The cut-off value of D* was $26.58 \times 10^{-3} \text{ mm}^2/\text{s}$. The findings suggest a relatively high tumor cellularity and hypervascularity^[13] caused by mutation of the KRAS oncogene^[29].

IVIM parameters correlated with histopathology of rectal tumor tissues. D values were more likely to correlate with cell count, Ki-67 index and total nucleic area. The f values showed good correlation with stained vessel area, total vessel area and vessel count. D* values correlated with mean vessel diameter^[33]. These findings confirmed that D reflected cell structure and water motion, and D* and f values reflect the vessel microenvironment^[11,13].

In rectal non-mucinous carcinoma and mucinous carcinoma, D, D* and f distinguished rectal tumor tissues from normal rectal wall, reflecting tumor tissue cellularity and microenvironment changes. Furthermore, lower f values were observed in poorly differentiated non-mucinous carcinoma and there were significant positive correlations with differentiation degree. This may be related to the fewer glands and glandular architecture in poorly differentiated tumors. D values were higher and D* values were lower in mucinous carcinomas than in non-mucinous carcinomas. Interestingly, correlation analysis showed D and D* had significant correlations with histological type. D was more likely to be related to cellular microstructure than to tumor cellularity^[11], and D* actually reflected blood flow and was affected by flow velocity and vascular geometry^[34]. IVIM-DWI-derived parameters were also useful for describing rectal tumor aggressiveness and prognosis^[31]. D* and f tended to increase with greater tumor differentiation, and D and D* decreased with advanced tumor stages. The f is the partial volume of the whole capillary vascular fraction^[9] and the proportion of the arterial blood is greater than the venous component for f at low b values^[35]. This phenomenon is reflected in well-differentiated tumors and poorly differentiated tumors: the capillary vascular network is relatively mature in the former, and there is poor structure of luminal vessels leading to low perfusion of the microcirculation in the latter^[31]. This could be confirmed by the correlation between the D*, f and MVD in colorectal tumors^[13]. Another important finding is that tumor invading the vascular wall had lower D* than did the group with no vascular wall invasion. This suggested that D* may be related to tumor stage. IVIM parameters were associated with some critical clinical indices, such as carcinoembryonic antigen (CEA) and CA199, which are related with prognosis^[31].

Another important application of IVIM-DWI is monitoring the therapeutic response. Sun *et al.*^[36] reported repeatability coefficients for 3.0T MRI in rectal cancer: correlations for D, f, and D* were 11.1%, 55.4%, and

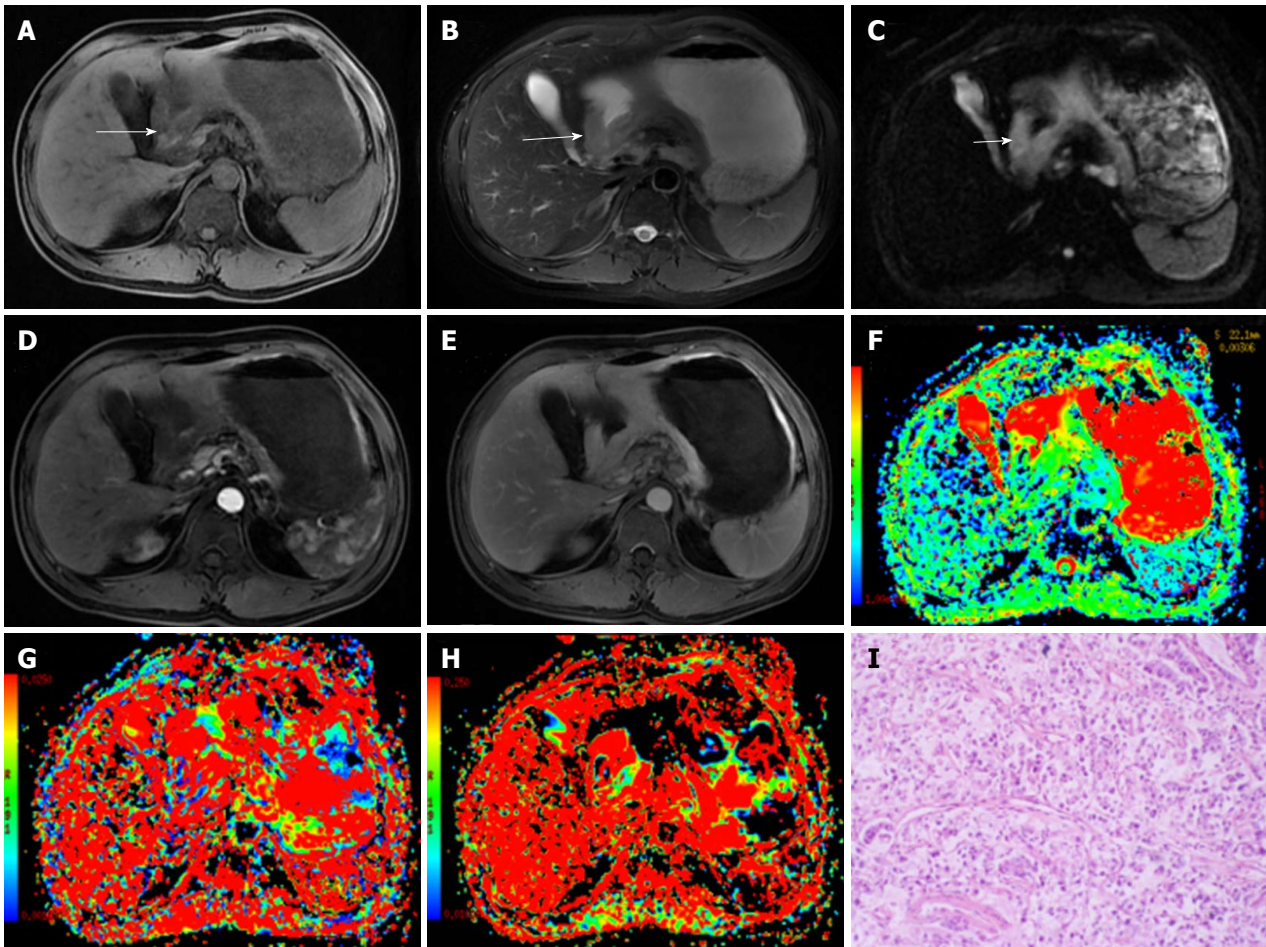


Figure 1 A 48-year-old male diagnosed with malignant gastric carcinoma (signet ring cell cancer). A, B: The lesion has slightly low signal on T1-weighted image (A) and slightly high signal intensity on T2-weighted image (B); C: On DWI, the cancer shows hyperintensity (white arrows); D, E: After contrast agent injection, the lesion shows mild-to-moderate enhancement in arterial and portal venous phases; F-H: The pseudocolor maps of D, D* and f derived from IVIM were displayed, the values of the D, D* and f are $0.92 \pm 0.11 \times 10^{-3} \text{ mm}^2/\text{s}$, $26.75 \pm 13.61 \times 10^{-3} \text{ mm}^2/\text{s}$ and $17.24\% \pm 4.8\%$, respectively; I: The HE staining of the tissues (100 \times).

40.3%, for intraobserver analysis, respectively, and were 41.6%, 134.0%, and 177.6%, for interobserver analysis, respectively. The test-retest repeatability coefficients for D, f, and D* were 24.5%, 126.3%, and 197.4%, respectively, larger than the intraobserver values. Therefore, D value showed better short-term test-retest reproducibility than did f or D*. The authors concluded that f and D* variance should be understood prudently in longitudinal studies on rectal cancer in which treatment response is monitored^[36]. In a report including 25 consecutive patients with advanced rectal carcinoma, D values were highest in the rectum ($1.29 \times 10^{-3} \text{ mm}^2/\text{s}$), then the tumor ($0.96 \times 10^{-3} \text{ mm}^2/\text{s}$) and fat ($0.37 \times 10^{-3} \text{ mm}^2/\text{s}$), and the f values were lower notably in tumor (9.12%) than in fat (16.05%) in patients not receiving neoadjuvant CRT. In patients receiving neoadjuvant CRT, D was higher in tumor ($1.10 \times 10^{-3} \text{ mm}^2/\text{s}$) and the rectum ($1.26 \times 10^{-3} \text{ mm}^2/\text{s}$) than in fat ($0.33 \times 10^{-3} \text{ mm}^2/\text{s}$).

For patients not receiving CRT, the vascular area fraction negatively correlated with D and positively correlated with f. For the rectum, D negatively correlated with cellularity C in patients after CRT^[11]. The

findings implied that D is related to tumor tissue activity that is frequently strongly vascularized^[37] and indicate the heterogeneous tumor tissue microenvironment. Furthermore, the correlation between D and cellularity C reflects the cellular microenvironment in the tumor, adjacent rectal wall and fat that affects water molecule Brownian motion directly^[11]. In another report with 31 patients with rectal cancer^[18], median D values increased remarkably pre- and post-CRT and were much higher in good responders to CRT. The median D was lower than the median ADC before and after CRT. The relative change was significantly greater in the good responders than in poor responders. Median D values showed higher AUCs than did ADC values for treatment response evaluation. This was because perfusion contributes to ADC in rectal cancer^[38] and microcirculation or perfusion effects can be identified by true tissue diffusion with sufficient b value sampling and bi-exponential curve fit analysis with IVIM^[9]. Nevertheless, median f and D* values change before and after CRT were not consistent with the degree of tumor response. This may be the limitation of D*, due to its high uncertainty and poor reproducibility^[39].

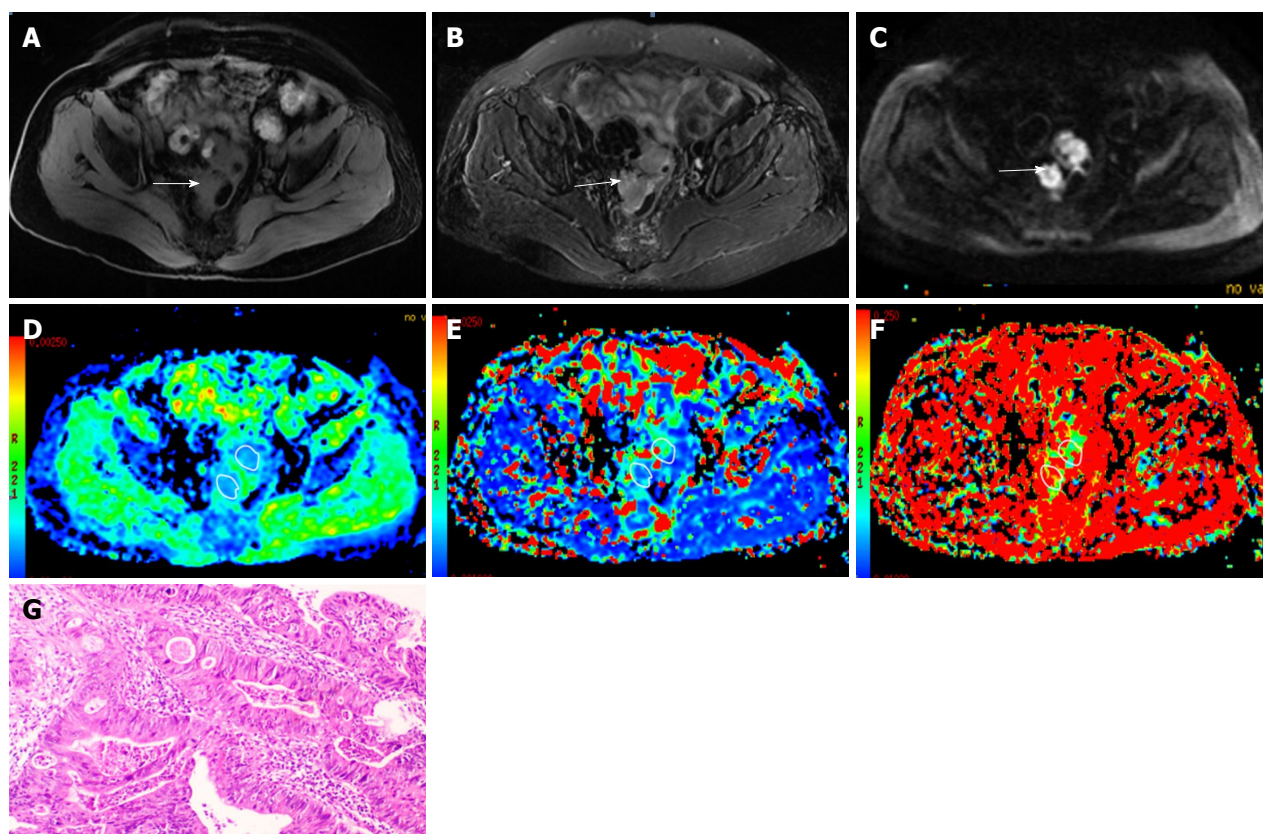


Figure 2 A 67-year-old female diagnosed as rectal cancer (poorly differentiated adenocarcinoma). A, B: The rectal cancer is isointense on T1-weighted image (A) with slightly high signal intensity on T2-weighted image (B); C: On diffusion weighted imaging, the cancer shows hyperintensity (white arrows); D-F: The pseudocolor maps of D, D* and f derived from intravoxel incoherent motion are displayed, the values of the D, D* and f were $1.03 \pm 0.12 \times 10^{-3} \text{mm}^2/\text{s}$, $50.35 \pm 24.96 \times 10^{-3} \text{mm}^2/\text{s}$ and $20.37\% \pm 5.9\%$, respectively; G: HE staining of the tissues (100 \times).

Similar results were reported by Lu *et al.*^[40] and Xu *et al.*^[41]. In these two studies, the IVIM-derived D value was a promising tool for predicting and identifying the pCR status prior to therapy. The D percentage changing values after therapy may be helpful and more accurate than traditional DWI for assessing pCR status.

Interestingly, in LARC before and after NACT, high tumor f was found to be useful for predicting better tumor response (tumor regression grade, TRG1-2) and the sensitivity and specificity was 69% and 100%, respectively. More importantly, f combined with tumor volume (fpre/Vpre) offered the best prediction of poor tumor response with a sensitivity of 88% and specificity of 91%, as well as 5-year progression-free survival (PFS) ($P < 0.01$)^[30]. These findings indicated that high f suggests tumor tissues with good vascular structures, and low f indicates poor vascular structures; and high f has been shown to be related to pathologic complete response (pCR)^[30] (Figure 2).

METASTATIC LESIONS

The parameters derived from IVIM-DWI are currently used for diagnosis of metastases, intra-tumor changes and therapeutic responses.

In metastasis diagnosis, IVIM-DWI may be useful in differentiating metastatic and non-metastatic lymph

nodes in patients with rectal carcinoma. In metastatic lymph nodes, because of the increased water molecular diffusion and microperfusion, reduced cellular density and increased tumor-related blood vessels within the metastatic lymph node, mean D and f values increased significantly, whereas mean D* values were lower than those of normal lymph nodes. The lower D* values may be due to the low blood velocity and MVD of tumor tissues at low b value ($< 200 \text{ s/mm}^2$)^[34]. Among the parameters, D values and D values combined with the short-axis diameter had the highest AUC, and D* values had the lowest^[34,42], suggesting that D is more sensitive and has the highest diagnostic efficacy in distinguishing normal from lymphatic metastasis^[15].

In assessment of therapeutic responses of metastatic lesions, parameters derived from IVIM-DWI changes are thought to be surrogate markers of tumor therapeutic responses. IVIM-DWI is usually sensitive to tumor necrosis after chemotherapy, because ADC in CRC metastases change along with specific increases in free molecular diffusion D that correlates with tumor necrosis^[43]. In another report, distant metastasis lesions had higher D* and relative perfusion (fD*) values, suggesting that IVIM parameters might reflect different clinical and histopathological features in rectal cancer^[33], although there were no significant differences between other IVIM parameters.

In patients with liver metastases from CRC treated with cytotoxic chemotherapy reported by Kim *et al.*^[44], after the first cycle of chemotherapy, ADC values increased ($1191.9 \pm 232.2 \times 10^{-3} \text{ mm}^2/\text{s}$ vs $1263.5 \pm 266.4 \times 10^{-3} \text{ mm}^2/\text{s}$; $P = 0.012$) and D ($1085.9 \pm 232.9 \times 10^{-3} \text{ mm}^2/\text{s}$ vs $1173.5 \pm 248.9 \times 10^{-3} \text{ mm}^2/\text{s}$; $P = 0.012$), while f values decreased ($173.7\% \pm 39.8\%$ vs $133.5\% \pm 28.3\%$; $P = 0.017$) in eight responding patients. In 24 responding metastatic lesions and 12 non-responding lesions after neoadjuvant FOLFIRI (5-FU, leucovorin, irinotecan) plus bevacizumab therapy, f values showed statistically significant differences between responder and non-responder lesions, and the f variation sensitivity and specificity were 62% and 93%, respectively^[45]. All findings indicated that IVIM-DWI and the parameters were useful for the prediction of therapeutic response after chemotherapy for metastases in CRC.

GASTROINTESTINAL STROMAL TUMORS

IVIM-DWI in gastrointestinal stromal tumors (GISTs) was also investigated to evaluate therapeutic responses to treatment with imatinib. In mice with xenografts bearing GIST-T1 cells, ADC values increased in the treated group. D* values in the treated group decreased significantly ($\Delta D^* = -41\%$, -49% , and -49%), and f increased significantly ($\Delta f = 79\%$, 82% and 110%) on days 1, 3 and 7 after treatment. D* and f did not show significant changes in the control group. The parameters from IVIM-DWI showed good correlation with histopathology with a decrease in cell proliferation and MVD and an increase in apoptosis and tumor necrosis in the treated group^[46]. Therefore, IVIM-DWI may serve as an effective imaging biomarker to assess GIST response to treatment.

CONCLUSION

It is a great challenge to evaluate and predict histopathological and therapeutic responses after GTs chemotherapy. IVIM, a new sequence derived from DWI, is a potentially useful tool for evaluation of GTs. The derived parameters D, D* and f reflect the micro-environment, microcirculation and blood flow changes in tumor tissues^[34], endowing them with the ability to predict tumor pathology and to monitor therapeutic responses. Therefore, the IVIM could offer a potentially accurate evaluation of chemotherapy efficacy, possibly facilitating individualized treatment planning in patients with GTs.

Encouragingly, based on the IVIM technique, more precise and effective parameters emerged for GTs, including α . The parameter α , derived from stretched-exponential model, appears to be more suitable for colorectal tumors in evaluating pCR after CRT because of the superior diagnostic performance of D, D* and f^[47] and their better reliability than ADC for assessing pCR after CRT.

In conclusion, with the technical assistance of IVIM, IVIM-DWI will be considerably more useful in evaluating GTs, reflecting histopathological changes and therapeutic responses before and after chemotherapy. Much deeper investigations and applications of IVIM-DWI in GTs are on the horizon.

REFERENCES

- 1 Torre LA, Bray F, Siegel RL, Ferlay J, Lortet-Tieulent J, Jemal A. Global cancer statistics, 2012. *CA Cancer J Clin* 2015; **65**: 87-108 [PMID: 25651787 DOI: 10.3322/caac.21262]
- 2 Siegel RL, Miller KD, Jemal A. Cancer statistics, 2018. *CA Cancer J Clin* 2018; **68**: 7-30 [PMID: 29313949 DOI: 10.3322/caac.21442]
- 3 Jang SH, Jung YJ, Kim MG, Kwon SJ. The Prognostic Significance of Compliance with Postoperative Adjuvant Chemotherapy in Patients with Stage III Gastric Cancer: an Observational Study. *J Gastric Cancer* 2018; **18**: 48-57 [PMID: 29629220 DOI: 10.5230/jgc.2018.18.e4]
- 4 Szafer A, Zhong J, Anderson AW, Gore JC. Diffusion-weighted imaging in tissues: theoretical models. *NMR Biomed* 1995; **8**: 289-296 [PMID: 8739267 DOI: 10.1002/nbm.1940080704]
- 5 Shinya S, Sasaki T, Nakagawa Y, Guiquing Z, Yamamoto F, Yamashita Y. The usefulness of diffusion-weighted imaging (DWI) for the detection of gastric cancer. *Hepatogastroenterology* 2007; **54**: 1378-1381 [PMID: 17708258]
- 6 Das A, Bhalla AS, Sharma R, Kumar A, Thakar A, Vishnubhatla SM, Sharma MC, Sharma SC. Can Diffusion Weighted Imaging Aid in Differentiating Benign from Malignant Sinonasal Masses?: A Useful Adjunct. *Pol J Radiol* 2017; **82**: 345-355 [PMID: 28740564 DOI: 10.12659/PJR.900633]
- 7 Hu F, Tang W, Sun Y, Wan D, Cai S, Zhang Z, Grimm R, Yan X, Fu C, Tong T, Peng W. The value of diffusion kurtosis imaging in assessing pathological complete response to neoadjuvant chemoradiation therapy in rectal cancer: a comparison with conventional diffusion-weighted imaging. *Oncotarget* 2017; **8**: 75597-75606 [PMID: 29088894 DOI: 10.18632/oncotarget.17491]
- 8 Thoeny HC, De Keyzer F, Vandecaveye V, Chen F, Sun X, Bosmans H, Hermans R, Verbeken EK, Boesch C, Marchal G, Landuyt W, Ni Y. Effect of vascular targeting agent in rat tumor model: dynamic contrast-enhanced versus diffusion-weighted MR imaging. *Radiology* 2005; **237**: 492-499 [PMID: 16192323 DOI: 10.1148/radiol.2372041638]
- 9 Le Bihan D, Breton E, Lallemand D, Aubin ML, Vignaud J, Laval-Jeantet M. Separation of diffusion and perfusion in intravoxel incoherent motion MR imaging. *Radiology* 1988; **168**: 497-505 [PMID: 3393671 DOI: 10.1148/radiology.168.2.3393671]
- 10 Cheng J, Wang Y, Zhang CF, Wang H, Wu WZ, Pan F, Hong N, Deng J. Chemotherapy response evaluation in a mouse model of gastric cancer using intravoxel incoherent motion diffusion-weighted MRI and histopathology. *World J Gastroenterol* 2017; **23**: 1990-2001 [PMID: 28373765 DOI: 10.3748/wjg.v23.i11.1990]
- 11 Bäuerle T, Seyler L, Münter M, Jensen A, Brand K, Fritzsche KH, Kopp-Schneider A, Schüssler M, Schlemmer HP, Stieltjes B, Ganten M. Diffusion-weighted imaging in rectal carcinoma patients without and after chemoradiotherapy: a comparative study with histology. *Eur J Radiol* 2013; **82**: 444-452 [PMID: 23219191 DOI: 10.1016/j.ejrad.2012.10.012]
- 12 Le Bihan DJ. Differentiation of benign versus pathologic compression fractures with diffusion-weighted MR imaging: a closer step toward the "holy grail" of tissue characterization? *Radiology* 1998; **207**: 305-307 [PMID: 9577472 DOI: 10.1148/radiology.207.2.9577472]
- 13 Lee HJ, Rha SY, Chung YE, Shim HS, Kim YJ, Hur J, Hong YJ, Choi BW. Tumor perfusion-related parameter of diffusion-weighted magnetic resonance imaging: correlation with histological microvessel density. *Magn Reson Med* 2014; **71**: 1554-1558 [PMID: 23798038 DOI: 10.1002/mrm.24810]
- 14 Jain RK, Duda DG, Willett CG, Sahani DV, Zhu AX, Loeffler JS,

- Batchelor TT, Sorensen AG. Biomarkers of response and resistance to antiangiogenic therapy. *Nat Rev Clin Oncol* 2009; **6**: 327-338 [PMID: 19483739 DOI: 10.1038/nrclinonc.2009.63]
- 15 **Qiu L**, Liu XL, Liu SR, Weng ZP, Chen XQ, Feng YZ, Cai XR, Guo CY. Role of quantitative intravoxel incoherent motion parameters in the preoperative diagnosis of nodal metastasis in patients with rectal carcinoma. *J Magn Reson Imaging* 2016; **44**: 1031-1039 [PMID: 27019309 DOI: 10.1002/jmri.25250]
- 16 **Zhu SC**, Liu YH, Wei Y, Li LL, Dou SW, Sun TY, Shi DP. Intravoxel incoherent motion diffusion-weighted magnetic resonance imaging for predicting histological grade of hepatocellular carcinoma: Comparison with conventional diffusion-weighted imaging. *World J Gastroenterol* 2018; **24**: 929-940 [PMID: 29491686 DOI: 10.3748/wjg.v24.i8.929]
- 17 **Iima M**, Kataoka M, Kanao S, Onishi N, Kawai M, Ohashi A, Sakaguchi R, Toi M, Togashi K. Intravoxel Incoherent Motion and Quantitative Non-Gaussian Diffusion MR Imaging: Evaluation of the Diagnostic and Prognostic Value of Several Markers of Malignant and Benign Breast Lesions. *Radiology* 2018; **287**: 432-441 [PMID: 29095673 DOI: 10.1148/radiol.2017162853]
- 18 **Nougaret S**, Vargas HA, Lakhman Y, Sudre R, Do RK, Bibeau F, Azria D, Assenat E, Molinari N, Pierredon MA, Rouanet P, Guiu B. Intravoxel Incoherent Motion-derived Histogram Metrics for Assessment of Response after Combined Chemotherapy and Radiation Therapy in Rectal Cancer: Initial Experience and Comparison between Single-Section and Volumetric Analyses. *Radiology* 2016; **280**: 446-454 [PMID: 26919562 DOI: 10.1148/radiol.2016150702]
- 19 **Federau C**. Intravoxel incoherent motion MRI as a means to measure in vivo perfusion: A review of the evidence. *NMR Biomed* 2017; **30** [PMID: 28885745 DOI: 10.1002/nbm.3780]
- 20 **Koh DM**, Collins DJ, Orton MR. Intravoxel incoherent motion in body diffusion-weighted MRI: reality and challenges. *AJR Am J Roentgenol* 2011; **196**: 1351-1361 [PMID: 21606299 DOI: 10.2214/AJR.10.5515]
- 21 **Ma L**, Xu X, Zhang M, Zheng S, Zhang B, Zhang W, Wang P. Dynamic contrast-enhanced MRI of gastric cancer: Correlations of the pharmacokinetic parameters with histological type, Lauren classification, and angiogenesis. *Magn Reson Imaging* 2017; **37**: 27-32 [PMID: 27840273 DOI: 10.1016/j.mri.2016.11.004]
- 22 **Di L**, Wu H, Zhu R, Li Y, Wu X, Xie R, Li H, Wang H, Zhang H, Xiao H, Chen H, Zhen H, Zhao K, Yang X, Xie M, Tuo B. Multi-disciplinary team for early gastric cancer diagnosis improves the detection rate of early gastric cancer. *BMC Gastroenterol* 2017; **17**: 147 [PMID: 29212444 DOI: 10.1186/s12876-017-0711-9]
- 23 **Hou F**, Shi DB, Chen YQ, Gao P. Human Epidermal Growth Factor Receptor-2 Promotes Invasion and Metastasis in Gastric Cancer by Activating Mitogen-activated Protein Kinase Signaling. *Appl Immunohistochem Mol Morphol* 2018 [PMID: 29734245 DOI: 10.1097/PAI.0000000000000672]
- 24 **Hwang GY**, Baek DW, Cho HJ, Lee SJ, Chae YS, Kang BW, Lee IH, Kim JG, Seo AN, Bae HI, Park KB, Park JY, Kwon OK, Lee SS, Chung HY. Elevated Neutrophil-to-Lymphocyte Ratio Predicts Survival in Patients with Advanced Gastric Cancer Treated with Trastuzumab Combination Chemotherapy. *Anticancer Res* 2018; **38**: 3151-3156 [PMID: 29715156 DOI: 10.21873/anticancer.12578]
- 25 **Ji C**, Zhang Q, Guan W, Guo T, Chen L, Liu S, He J, Zhou Z. Role of intravoxel incoherent motion MR imaging in preoperative assessing HER2 status of gastric cancers. *Oncotarget* 2017; **8**: 49293-49302 [PMID: 28514733 DOI: 10.18632/oncotarget.17570]
- 26 **Song XL**, Kang HK, Jeong GW, Ahn KY, Jeong YY, Kang YJ, Cho HJ, Moon CM. Intravoxel incoherent motion diffusion-weighted imaging for monitoring chemotherapeutic efficacy in gastric cancer. *World J Gastroenterol* 2016; **22**: 5520-5531 [PMID: 27350730 DOI: 10.3748/wjg.v22.i24.5520]
- 27 **Zhang G**, Wang S, Wen D, Zhang J, Wei X, Ma W, Zhao W, Wang M, Wu G, Zhang J. Comparison of non-Gaussian and Gaussian diffusion models of diffusion weighted imaging of rectal cancer at 3.0 T MRI. *Sci Rep* 2016; **6**: 38782 [PMID: 27934928 DOI: 10.1038/srep38782]
- 28 **Fusco R**, Sansone M, Petrillo A. A comparison of fitting algorithms for diffusion-weighted MRI data analysis using an intravoxel incoherent motion model. *MAGMA* 2017; **30**: 113-120 [PMID: 27670762 DOI: 10.1007/s10334-016-0591-y]
- 29 **Xu Y**, Xu Q, Sun H, Liu T, Shi K, Wang W. Could IVIM and ADC help in predicting the KRAS status in patients with rectal cancer? *Eur Radiol* 2018; **28**: 3059-3065 [PMID: 29450716 DOI: 10.1007/s00330-018-5329-y]
- 30 **Bakke KM**, Hole KH, Dueland S, Grøholt KK, Flatmark K, Ree AH, Seierstad T, Redalen KR. Diffusion-weighted magnetic resonance imaging of rectal cancer: tumour volume and perfusion fraction predict chemoradiotherapy response and survival. *Acta Oncol* 2017; **56**: 813-818 [PMID: 28464745 DOI: 10.1080/0284186X.2017.1287951]
- 31 **Sun H**, Xu Y, Song A, Shi K, Wang W. Intravoxel Incoherent Motion MRI of Rectal Cancer: Correlation of Diffusion and Perfusion Characteristics With Prognostic Tumor Markers. *AJR Am J Roentgenol* 2018; **210**: W139-W147 [PMID: 29446674 DOI: 10.2214/AJR.17.18342]
- 32 **Itoh N**, Ohta K, Ohta M, Kawasaki T, Yamashina I. The nucleotide sequence of a gene for a putative ribosomal protein S31 of Drosophila. *Nucleic Acids Res* 1989; **17**: 2121 [PMID: 2928115 DOI: 10.1093/nar/17.5.2121]
- 33 **Surov A**, Meyer HJ, Höhn AK, Behrmann C, Wienke A, Spielmann RP, Garnov N. Correlations between intravoxel incoherent motion (IVIM) parameters and histological findings in rectal cancer: preliminary results. *Oncotarget* 2017; **8**: 21974-21983 [PMID: 28423540 DOI: 10.18632/oncotarget.15753]
- 34 **Lu B**, Yang X, Xiao X, Chen Y, Yan X, Yu S. Intravoxel Incoherent Motion Diffusion-Weighted Imaging of Primary Rectal Carcinoma: Correlation with Histopathology. *Med Sci Monit* 2018; **24**: 2429-2436 [PMID: 29679528 DOI: 10.12659/MSM.908574]
- 35 **Duong TQ**, Kim SG. In vivo MR measurements of regional arterial and venous blood volume fractions in intact rat brain. *Magn Reson Med* 2000; **43**: 393-402 [PMID: 10725882 DOI: 10.1002/(SICI)1522-2594(200003)43:3<393::AID-MRM11>3.0.CO;2-K]
- 36 **Sun H**, Xu Y, Xu Q, Shi K, Wang W. Rectal cancer: Short-term reproducibility of intravoxel incoherent motion parameters in 3.0T magnetic resonance imaging. *Medicine (Baltimore)* 2017; **96**: e6866 [PMID: 28489784 DOI: 10.1097/MD.00000000000006866]
- 37 **Baeriswyl V**, Christofori G. The angiogenic switch in carcinogenesis. *Semin Cancer Biol* 2009; **19**: 329-337 [PMID: 19482086 DOI: 10.1016/j.semcancer.2009.05.003]
- 38 **Woo S**, Lee JM, Yoon JH, Joo I, Han JK, Choi BI. Intravoxel incoherent motion diffusion-weighted MR imaging of hepatocellular carcinoma: correlation with enhancement degree and histologic grade. *Radiology* 2014; **270**: 758-767 [PMID: 24475811 DOI: 10.1148/radiol.13130444]
- 39 **Kakite S**, Dyvorne H, Besa C, Cooper N, Facciuto M, Donnerhack C, Taouli B. Hepatocellular carcinoma: short-term reproducibility of apparent diffusion coefficient and intravoxel incoherent motion parameters at 3.0T. *J Magn Reson Imaging* 2015; **41**: 149-156 [PMID: 24415565 DOI: 10.1002/jmri.24538]
- 40 **Lu W**, Jing H, Ju-Mei Z, Shao-Lin N, Fang C, Xiao-Ping Y, Qiang L, Biao Z, Su-Yu Z, Ying H. Intravoxel incoherent motion diffusion-weighted imaging for discriminating the pathological response to neoadjuvant chemoradiotherapy in locally advanced rectal cancer. *Sci Rep* 2017; **7**: 8496 [PMID: 28819296 DOI: 10.1038/s41598-017-09227-9]
- 41 **Xu Q**, Xu Y, Sun H, Chan Q, Shi K, Song A, Wang W. Quantitative intravoxel incoherent motion parameters derived from whole-tumor volume for assessing pathological complete response to neoadjuvant chemotherapy in locally advanced rectal cancer. *J Magn Reson Imaging* 2018; **48**: 248-258 [PMID: 29281151 DOI: 10.1002/jmri.25931]
- 42 **Yu XP**, Wen L, Hou J, Bi F, Hu P, Wang H, Wang W. Discrimination between Metastatic and Nonmetastatic Mesorectal Lymph Nodes in Rectal Cancer Using Intravoxel Incoherent Motion Diffusion-weighted Magnetic Resonance Imaging. *Acad Radiol* 2016; **23**: 479-485 [PMID: 26853971 DOI: 10.1016/j.acra.2015.12.013]

- 43 **Chiaradia M**, Baranes L, Van Nhieu JT, Vignaud A, Laurent A, Decaens T, Charles-Nelson A, Brugières P, Katsahian S, Djabbari M, Deux JF, Sobhani I, Karoui M, Rahmouni A, Luciani A. Intravoxel incoherent motion (IVIM) MR imaging of colorectal liver metastases: are we only looking at tumor necrosis? *J Magn Reson Imaging* 2014; **39**: 317-325 [PMID: 23723012 DOI: 10.1002/jmri.24172]
- 44 **Kim JH**, Joo I, Kim TY, Han SW, Kim YJ, Lee JM, Han JK. Diffusion-Related MRI Parameters for Assessing Early Treatment Response of Liver Metastases to Cytotoxic Therapy in Colorectal Cancer. *AJR Am J Roentgenol* 2016; **207**: W26-W32 [PMID: 27303858 DOI: 10.2214/AJR.15.15683]
- 45 **Granata V**, Fusco R, Catalano O, Filice S, Amato DM, Nasti G, Avallone A, Izzo F, Petrillo A. Early Assessment of Colorectal Cancer Patients with Liver Metastases Treated with Antiangiogenic Drugs: The Role of Intravoxel Incoherent Motion in Diffusion-Weighted Imaging. *PLoS One* 2015; **10**: e0142876 [PMID: 26566221 DOI: 10.1371/journal.pone.0142876]
- 46 **Pan F**, Den J, Zhang C, Wang H, Cheng J, Wu W, Hong N, Wang Y. The Therapeutic Response of Gastrointestinal Stromal Tumors to Imatinib Treatment Assessed by Intravoxel Incoherent Motion Diffusion-Weighted Magnetic Resonance Imaging with Histopathological Correlation. *PLoS One* 2016; **11**: e0167720 [PMID: 27911930 DOI: 10.1371/journal.pone.0167720]
- 47 **Zhu HB**, Zhang XY, Zhou XH, Li XT, Liu YL, Wang S, Sun YS. Assessment of pathological complete response to preoperative chemoradiotherapy by means of multiple mathematical models of diffusion-weighted MRI in locally advanced rectal cancer: A prospective single-center study. *J Magn Reson Imaging* 2017; **46**: 175-183 [PMID: 27981667 DOI: 10.1002/jmri.25567]

P- Reviewer: Cao D, Ciocalteu A, Hori T, Mastoraki A

S- Editor: Ji FF **L- Editor:** A **E- Editor:** Wu YXJ



Observational Study

Reproducibility of thrombus volume quantification in multicenter computed tomography pulmonary angiography studies

Audrey E Kaufman, Alison N Pruzan, Ching Hsu, Sarayu Ramachandran, Adam Jacobi, Indravadan Patel, Lee Schwocho, Michele F Mercuri, Zahi A Fayad, Venkatesh Mani

Audrey E Kaufman, Alison N Pruzan, Sarayu Ramachandran, Adam Jacobi, Indravadan Patel, Lee Schwocho, Michele F Mercuri, Zahi A Fayad, Venkatesh Mani, Department of Radiology, Icahn School of Medicine at Mount Sinai, New York, NY 10029, United States

Audrey E Kaufman, Alison N Pruzan, Sarayu Ramachandran, Zahi A Fayad, Venkatesh Mani, Translational and Molecular Imaging Institute, Icahn School of Medicine at Mount Sinai, Hess Center for Science and Medicine, New York, NY 10029, United States

Ching Hsu, Indravadan Patel, Lee Schwocho, Michele F Mercuri, Daiichi Sankyo Inc., Basking Ridge, NJ 07920, United States

ORCID number: Audrey E Kaufman (0000-0002-9221-9004); Alison N Pruzan (0000-0002-3054-6341); Ching Hsu (0000-0003-0616-2468); Sarayu Ramachandran (0000-0002-9917-5876); Adam Jacobi (0000-0002-9057-9129); Indravadan Patel (0000-0001-6138-0850); Lee Schwocho (0000-0002-3030-799X); Michele F Mercuri (0000-0003-2266-4812); Zahi A Fayad (0000-0002-3439-7347); Venkatesh Mani (0000-0002-0432-2918).

Author contributions: All authors designed the experiment; Kaufman AE, Pruzan AN, Ramachandran S, Mani V performed the experiment; Kaufman AE and Pruzan AN performed the image analysis; Hsu C, Pruzan AN and Mani V performed statistical analysis; Kaufman AE and Mani V wrote the draft of the manuscript; all authors critically reviewed the manuscript.

Institutional review board statement: This study was submitted to the Institutional Review Board (IRB) of the Icahn School of Medicine at Mount Sinai but was deemed that no IRB approval was necessary for conduct of this study [See Determination regarding engagement in human research letter from the program for protection of research subjects (PPHS) office IRB].

Informed consent statement: Waiver of informed consent was obtained from the Institutional Review Board as only deidentified data was used in this study. The images analyzed for this study

were anonymized and devoid of any Protected Health Information.

Conflict-of-interest statement: Ching Hsu, Indravadan Patel, Lee Schwocho, Michele F Mercuri are employees of Daiichi Sankyo Inc. All other authors have no conflicts to disclose.

Data sharing statement: Once published and after appropriate safeguard to ensure that the data is devoid of any identifiers, the data used for the analysis for this study will be shared on the Mount Sinai data sharing portal according to Institutional guidelines.

STROBE Statement: The authors have read the STROBE Statement - checklist of items, and the manuscript was prepared and revised according to the STROBE Statement - checklist of items.

Open-Access: This article is an open-access article which was selected by an in-house editor and fully peer-reviewed by external reviewers. It is distributed in accordance with the Creative Commons Attribution Non Commercial (CC BY-NC 4.0) license, which permits others to distribute, remix, adapt, build upon this work non-commercially, and license their derivative works on different terms, provided the original work is properly cited and the use is non-commercial. See: <http://creativecommons.org/licenses/by-nc/4.0/>

Manuscript source: Invited Manuscript

Correspondence to: Venkatesh Mani, PhD, Associate Professor, Department of Radiology, Icahn School of Medicine at Mount Sinai, 1470 Madison Avenue, New York, NY 10029, United States. venkatesh.mani@mountsinai.org
Telephone: +1-212-8248454
Fax: +1-646-5379589

Received: June 1, 2018

Peer-review started: June 1, 2018

First decision: July 23, 2018

Revised: July 27, 2018

Accepted: August 4, 2018

Article in press: August 4, 2018

Published online: October 28, 2018

Abstract

AIM

To evaluate reproducibility of pulmonary embolism (PE) clot volume quantification using computed tomography pulmonary angiogram (CTPA) in a multicenter setting.

METHODS

This study was performed using anonymized data in conformance with HIPAA and IRB Regulations (March 2015–November 2016). Anonymized CTPA data was acquired from 23 scanners from 18 imaging centers using each site's standard PE protocol. Two independent analysts measured PE volumes using a semi-automated region-growing algorithm on an FDA-approved image analysis platform. Total thrombus volume (TTV) was calculated per patient as the primary endpoint. Secondary endpoints were individual thrombus volume (ITV), Qanadli score and modified Qanadli score per patient. Inter- and intra-observer reproducibility were assessed using intra-class correlation coefficient (ICC) and Bland-Altman analysis.

RESULTS

Analyst 1 found 72 emboli in the 23 patients with a mean number of emboli of 3.13 per patient with a range of 0–11 emboli per patient. The clot volumes ranged from 0.0041 – 47.34 cm³ (mean \pm SD, 5.93 \pm 10.15cm³). On the second read, analyst 1 found the same number and distribution of emboli with a range of volumes for read 2 from 0.0041 – 45.52 cm³ (mean \pm SD, 5.42 \pm 9.53cm³). Analyst 2 found 73 emboli in the 23 patients with a mean number of emboli of 3.17 per patient with a range of 0–11 emboli per patient. The clot volumes ranged from 0.00459–46.29 cm³ (mean \pm SD, 5.91 \pm 10.06 cm³). Inter- and intra-observer variability measurements indicated excellent reproducibility of the semi-automated method for quantifying PE volume burden. ICC for all endpoints was greater than 0.95 for inter- and intra-observer analysis. Bland-Altman analysis indicated no significant biases.

CONCLUSION

Semi-automated region growing algorithm for quantifying PE is reproducible using data from multiple scanners and is a suitable method for image analysis in multicenter clinical trials.

Key words: Pulmonary embolism; Arteries; Computed tomography angiography; Computer-assisted image analysis; Thrombolytic therapy

© **The Author(s) 2018.** Published by Baishideng Publishing Group Inc. All rights reserved.

Core tip: Blood clots that occur in deep leg veins can break away and cause the serious complication of clots

(then termed emboli) lodged in the lungs. Measuring the volume of the emboli with a semi-automated region growing software program using computed tomography pulmonary angiogram data can be helpful to evaluate treatment efficacy in clinical drug trials. This study demonstrates the technique to be reproducible both between image analysts and when repeated by the same image analyst when the data is obtained in a multicenter setting.

Kaufman AE, Pruzan AN, Hsu C, Ramachandran S, Jacobi A, Patel I, Schwocho L, Mercuri MF, Fayad ZA, Mani V. Reproducibility of thrombus volume quantification in multicenter computed tomography pulmonary angiography studies. *World J Radiol* 2018; 10(10): 124-134 Available from: URL: <http://www.wjgnet.com/1949-8470/full/v10/i10/124.htm> DOI: <http://dx.doi.org/10.4329/wjr.v10.i10.124>

INTRODUCTION

Venous thromboembolism (VTE) represents the combined disease states of deep venous thrombosis (DVT) and pulmonary embolism (PE). PE is the most significant sequela of DVT, occurring in more than a third of DVT patients^[1]. In the United States, there is a combined average annual incidence of over 275000 new cases of VTE among whites of predominantly European origin and African-Americans^[2]. A retrospective study demonstrated an incidence of 117 VTE cases per 100000 in a demographically white population^[3]. The same study showed VTE to be predominantly a disease of older age, with males slightly more affected than females, whereas in the younger population the incidence is higher in females during child-bearing age^[3].

PE has a high mortality rate^[4,5]. The two week and three month post diagnosis all-cause mortality rate was found to be 11.4% and 17.4% respectively^[6]. Risk of mortality in PE rests upon multiple factors including clinical findings of shock and hypotension and elevated markers of right ventricular dysfunction and myocardial injury^[7,8]. Clot burden alone is not a principal marker in clinical risk stratification, however computed tomography pulmonary angiogram (CTPA), is a commonly used diagnostic tool that has been shown to help with risk stratification of PE^[9-11]. Objectively measuring thrombus volume from CTPA data can be particularly useful to evaluate the efficacy of treatments for PE^[12]. Indeed, clinical pharmaceutical trials of drugs such as thrombolytics rely upon objective measures including total thrombus volume (TTV), the sum of volumes of all PE present in an individual, to assess drug effectiveness and potency and to help determine the optimal duration of therapy^[13]. This study is not performed to assess CTPA measured clot volumes as a clinical prognostic indicator. Rather, the goal of this study is to evaluate the reproducibility of a quantifiable metric; the TTV in PE, especially as new drugs are being developed that

aim to eliminate and reduce clot size. Thrombus volume measured by contrast enhanced CTPA could potentially serve as an imaging biomarker for evaluating burden and/or severity of PE in clinical trials. One such current study is the DS-1040b, a Randomized Study to Assess the Safety, Pharmacokinetics/Dynamics of DS-1040b in Subjects With Acute Submassive Pulmonary Embolism, NCT02923115 (www.clinicaltrials.gov).

Quantifying clot burden with CTPA requires segmentation of emboli from non-thrombotic contrast-enhanced blood within the pulmonary vasculature and computation of clot volume. Semi-automated region growing algorithms can be used for this purpose^[12]. The inter and intra-observer reliability of this technique has been tested in data obtained from a single center using one fixed CTPA imaging protocol^[12]. Accuracy of this approach has also been established by the relative volume measurement error^[12]. However, these types of studies have not been implemented in a multicenter setting. This is a retrospective study performed on sample data obtained from subjects undergoing CT pulmonary angiography for suspected PE. Images were obtained from multiple centers as part of a study qualification visit for a multicenter drug trial evaluating a new thrombolytic agent and were from cases of suspected PE at the site obtained in the week prior to the qualification visit. Therefore, in addition to the stated study goal of evaluating the quantifiable metric of TTV in PE, the broader purpose of this study is to evaluate the hypothesis that repeatable volume quantification can be made using a semi-automated region growing algorithm on *in vivo* PE data obtained in a multicenter setting with inherent variability of CT scanners and acquisition and reconstruction parameters using TTV as a primary endpoint and individual thrombus volume (ITV), Qanadli score and modified Qanadli score as secondary endpoints.

MATERIALS AND METHODS

This study was performed using anonymized data in conformance with HIPAA and IRB Regulations (March 2015-November 2016).

CTPA data was acquired from 23 scanners from 18 different centers using the standard image acquisition for PE at the site. Table 1 describes the image acquisition and reconstruction parameters and contrast agent use protocol at each center. The data was completely anonymized. Patient demographic data was not included in the study as the cases obtained from the multicenter sites were requested as part of our core lab qualification assessment for participation in a clinical pharmaceutical trial, and as such, a deidentified random sample case(s) from each site was requested. From image metadata, limited information on gender and/or age on less than half of the cases were determined. No other demographic information was available to the authors. Of the 23 patients studied, seven were known to be male. Where the male's age was identified the following ages were

known: 72, 60, 82, 30 and 73. Two patients were known to be female where their ages were known to be 21 and 77. There were also two patients of unknown gender that were known to be 72 and 81 years old.

Two experienced image analysts performed the *in vivo* study. AEK (a board-certified diagnostic radiologist with six years clinical experience) and ANP (Bachelor of Science with two years vascular imaging experience under the supervision of board certified radiologists (AJ, AEK) assessed each patient for the presence of emboli within the pulmonary arterial tree. The extent of the analysis was from the main pulmonary artery up to and including emboli within segmental arteries bilaterally. See Figure 1 for a schematic of the segmental distribution of the pulmonary arteries. An embolus appeared as a filling defect of soft tissue density within the otherwise contrast enhanced pulmonary arterial tree. An endoluminal filling defect was deemed a single embolus if it was contiguous and demonstrated no intervening contrast material fully separating it from adjacent clot. Embolus volume was the measured parameter and the endpoints were TTV and ITV in each patient and both the Qanadli and modified Qanadli score in all patients. Each separate embolus was analyzed using a semi-automated region growing algorithm implemented in the FDA approved Siemens *syngo.via* image analysis platform. This region growing algorithm was similar to what has been used in previous studies for quantification of PE clot volume^[12] and was also based on the methods shown in the following papers^[14-16]. Briefly, the region growing algorithm was a pixel-based image segmentation approach involving the initial selection of seed points by the user. This segmentation method examined the nearest neighboring pixels of initial seed points and determined if the pixel neighbors should be added to the region. The process was then iterated on, using data clustering algorithms based on image pixel data intensity and texture.

At the viewing workstation, the image analyst performed segmentation and volumetric quantification of emboli. To acquire these readings, the cursor was placed on the clot and the left mouse button was pressed and held in order to grow into adjacent regions with similar density readings. The analyst then assessed the need to include and/or exclude portions of the segmented mask by visually assessing the anatomic extent of the embolus and the surrounding anatomic structures and then made appropriate corrections and adjustments to the segmented mask. Figure 2 shows an example of *in vivo* region growing. In order to determine the inter observer reproducibility of the data analysis, the two independent observers were blinded to each other's interpretations when computing the dot volumes for each of the datasets using the same semi-automated algorithm and image analysis package^[12,14-16]. One reader (AEK) repeated the analysis a second time to establish the intra-reader reproducibility.

A Qanadli score was calculated by assessing the presence and degree of obstruction in the pulmonary

Table 1 Scanner Information and computed tomography pulmonary angiogram acquisition protocol from each scanner

| Site | Scan | Manufacturer | Model | Number of slices | Recon thickness (mm) | kVp | Pitch | Contrast agent |
|---|------|--------------|--------------------|------------------|----------------------|-----|----------|----------------|
| Academic Medical Center, Amsterdam, Netherlands | 1 | Siemens | Definition AS+ | 128 | 1 | 120 | 0.45 | Ultravist 300 |
| | 2 | Siemens | Force | 384 | 1.5 | 90 | 0.55 | Ultravist 300 |
| Azienda Ospedaliero Universitaria Ospedali Riuniti Di Ancona, Ancona, Italy | 3 | Philips | Brilliance 16 | 16 | 2 | 120 | 0.9 | Isovue 350 |
| Fondazione Poliambulanza Istituto Ospedaliero, Brescia, Italy | 4 | GE | Optima CT660 | 128 | 0.625 | 120 | 1.375 | Ultravist 370 |
| Hôpital de la Cavale Blanche, Brest, France | 5 | Siemens | Definition AS + | 128 | 1 | 100 | 1.2 | Iomeron 400 |
| Cliniques Universitaires Saint-Luc, Brussels, Belgium | 6 | Philips | ICT Brilliance 64 | 256 | 1 | 120 | 0.797 | Iomeron 400 |
| CHU de Clermont-Ferrand, Clermont-Ferrand, France | 7 | GE | Revolution GSI | 64 | 0.625 | 120 | 1.375 | Ultravist 370 |
| Hospital Universitario Dr. Josep Trueta, Girona, Spain | 8 | Philips | Ingenuity CT | 64 | 1 | 120 | 0.952 | Omnipaque 350 |
| Medical University Graz, Graz, Austria | 9 | Toshiba | Aquilion64 | 64 | 0.5 | 120 | 1 | Optiray 350 |
| Universitätsmedizin Greifswald, Greifswald, Germany | 10 | Toshiba | Aquilion64 | 64 | 0.5 | 120 | 1 | Iomeron 400 |
| | 11 | Siemens | Sensation 16 | 16 | 1.5 | 120 | 1.2 | Iomeron 350 |
| Hopital Michallon - CHUGA, Grenoble, France | 12 | GE | Optima CT 660 | 128 | 0.625 | 100 | 0.984375 | Iomeron 350 |
| Leiden University Medical Center, Leiden, Netherlands | 13 | Toshiba | Aquilion ONE | 320 | 1 | 80 | 0.8129 | Ultravist 370 |
| UZ Gasthuisberg, Leuven, Belgium | 14 | Siemens | Definition Flash | 128 | 1 | 100 | 0.55 | Visipaque 320 |
| | 15 | Siemens | Definition Flash | 128 | 1 | 100 | 0.55 | Visipaque 320 |
| | 16 | Siemens | Definition Flash | 128 | 1 | 100 | 0.55 | Visipaque 320 |
| Cedars Sinai Medical Center, Los Angeles, United States | 17 | GE | LightSpeed VCT | 64 | 0.625 | 120 | 0.984375 | Omnipaque 350 |
| Hospital Universitario Ramon y Cajal, Madrid, Spain | 18 | Toshiba | Aquilion ONE | 320 | 0.5 | 100 | 1.375 | Iomeron 350 |
| Intercoastal Medical Group, Sarasota, United States | 19 | Siemens | Definition AS+ | 128 | 0.6 | 120 | 1.1 | Isovue 370 |
| CHU de St. Etienne, St. Etienne, France | 20 | Siemens | Definition DS | 64 | 1 | 120 | 1.2 | Xenetix 350 |
| Strasbourg University Hospital, Strasbourg, France | 21 | GE | Discovery CT750 HD | 64 | 0.625 | 100 | 1.375 | Iomeron 400 |
| Ospedale di Circolo, University of Insubria, Varese, Italy | 22 | Toshiba | Aquilion One | 320 | 1 | 100 | 0.8129 | Iomeron 400 |
| | 23 | Siemens | Sensation 40 | 40 | 0.75 | 100 | 1 | Iomeron 370 |

All images were obtained with dose modulation of tube current. Filter and reconstruction kernels varied.

arterial tree bilaterally^[17]. More specifically, the Qanadli score was calculated by assessing the CTPA in two ways, first, by evaluating the distribution of emboli in order to arrive at a weighting factor, and second, by determining a level of occlusion score. There are 10 segmental arteries on each side with three segmental arteries feeding the upper lobes, two feeding the right middle lobe and lingula (left) and five feeding the lower lobes. The presence of an embolus in a segmental vessel was given a weighting score of one. Central arteries were given heavier weighting than more distal vessels using the following method: the weighting factor for a vessel with an embolus was based on the number of segmental vessels it feeds. The more distal vessels were then excluded from the score. The scale for the

level of obstruction of a given vessel was as follows: 0 represents no embolus detected; 1 represents a partially occlusive embolus; and 2 represent a fully occlusive embolus. When the weighting factor and obstruction factors were multiplied then added together, there was a maximal possible score of 20 per side for a total possible raw score of 40. With this information the Qanadli score was then calculated and reported as a percentage by dividing the raw score by 40, the maximal score^[17].

A Modified Qanadli score was also calculated by solely assessing the presence and degree of obstruction in the ten segmental vessels bilaterally^[18]. We performed this additional obstruction index to pull out any difference that may be seen by using the

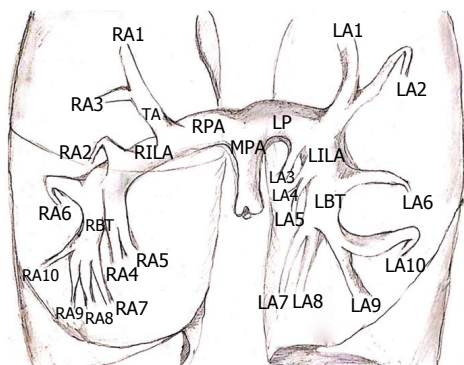


Figure 1 Schematic of segmental distribution of pulmonary arteries. MPA: Main pulmonary artery; RPA: Right pulmonary artery; TA: Truncus anterior; RILA: Right interlobar artery; RBT: Right basal trunk; RA1: Right upper lobe, apical; RA2: Right upper lobe, posterior; RA3: Right upper lobe, anterior; RA4: Right middle lobe, lateral; RA5: Right middle lobe, medial; RA6: Right lower lobe, superior; RA7: Right lower lobe, medial basal; RA8: Right lower lobe, anterior basal; RA9: Right lower lobe, lateral basal; RA10: Right lower lobe, posterior basal; LPA: Left pulmonary artery; LILA: Left interlobar artery; LBT: Left basal trunk; LA1: Left upper lobe, apical; LA2: Left upper lobe, posterior; LA3: Left upper lobe, anterior; LA4: Lingula, superior; LA5: Lingula, inferior; LA6: Left lower lobe, superior; LA7: Left lower lobe, medial basal; LA8: Left lower lobe, anterior basal; LA9: Left lower lobe, lateral basal; LA10: Left lower lobe, posterior basal.

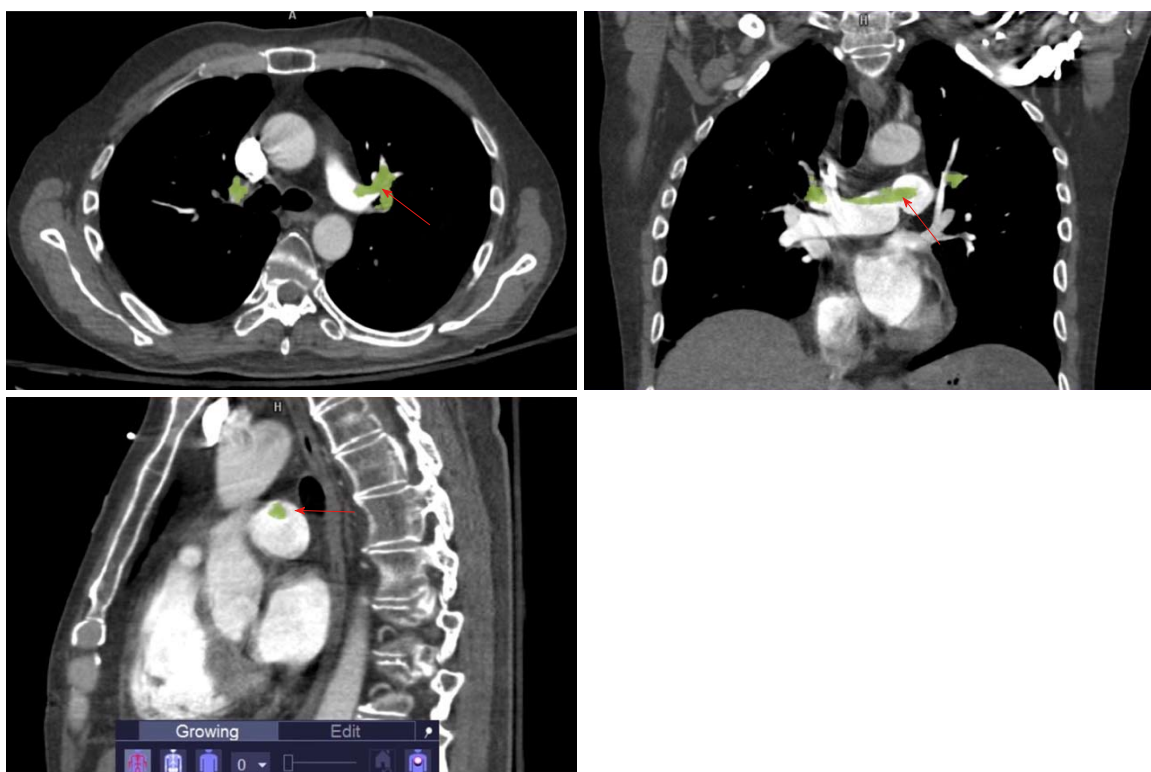


Figure 2 Computed tomography pulmonary angiogram images demonstrating segmentation of a saddle embolus in three orthogonal views (arrows).

Qanadli with its focus on weighted central vessels vs simply assessing obstruction in the individual segmental vessels alone as we have done in our modified version. The same Qanadli scale for the level of obstruction was used in our modified version with 0 representing no embolus, 1 representing a partially occlusive embolus, and 2 representing a fully occlusive embolus. As with Qanadli scoring, a maximum raw score of 40 and a final score reported as a percentage relative to 40 was used.

Statistical analysis

All statistical analysis presented here was performed or

guided by a biomedical statistician. Intra-class correlation coefficients (ICCs) and Bland-Altman analyses were performed using GraphPad Prism 7 for Mac, GraphPad Software, San Diego California, United States, www.graphpad.com. The ICCs were used to compare the results obtained between the two readers as well as to compare the results obtained from the two analyses of the same reader. The agreement between the measurements by each observer in the two reading sessions and the agreement between the two observers were also assessed using Bland-Altman analyses. According to this method, the mean difference between

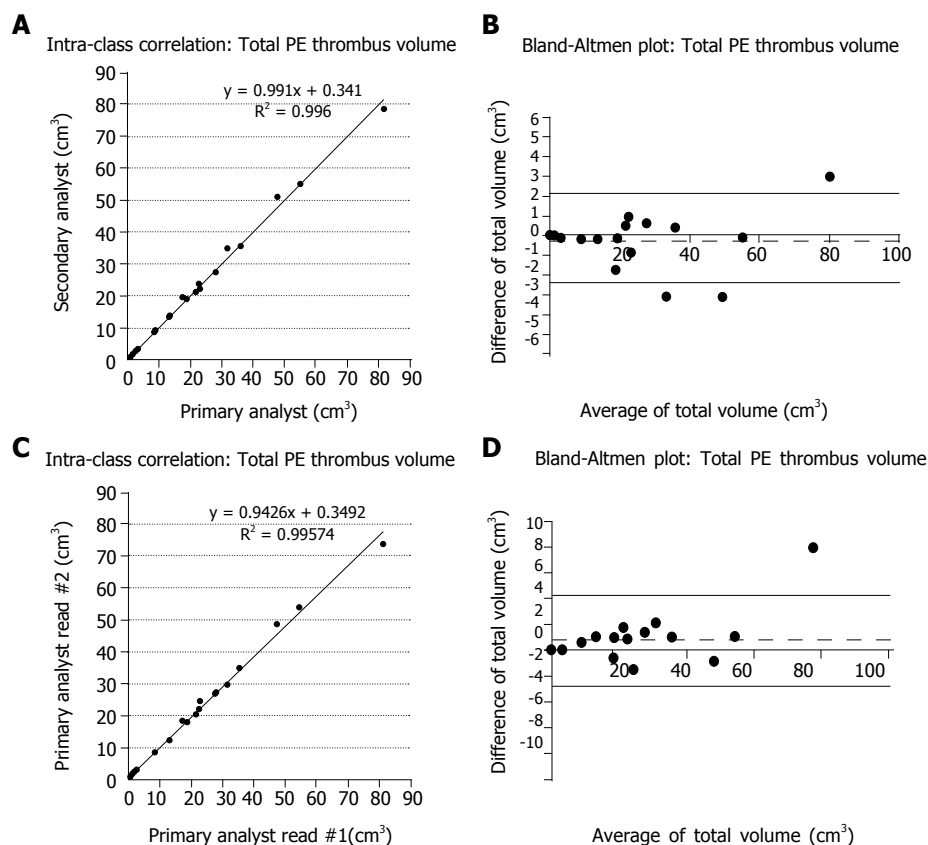


Figure 3 Total thrombus volume inter- and intra-observer reproducibility (A) Intra-class correlation coefficient (ICC) plot and (B) Bland Altman plot comparing the total PE thrombus volume results of the primary and secondary image analyst for the inter-observer reproducibility analysis (C) ICC plot and (D) Bland Altman plot comparing the total pulmonary embolism thrombus volume results of the first and second read of the primary image analyst for the intra-observer reproducibility analysis.

measurements is defined as “bias” and represents the systemic error in measurements. We calculated 95%CI for bias and for the limits of agreement. ICC provides the overall inter- or intra-observer agreement whereas the Bland-Altman method gives the discrepancy in measurements at the individual level. A one sample *t*-test was performed to determine if any bias was observed on the Bland-Altman analysis. For TTV, in addition to evaluating absolute differences by Bland Altman analysis, we also evaluated the % difference between the two readers or two reads.

RESULTS

Analyst 1 found 72 emboli in the 23 patients with a mean number of emboli of 3.13 per patient. With the three negative cases excluded the mean number of emboli per patient was 3.6. Considering all cases there was a range of 0-11 emboli per patient. (0 in 3 patients (pts); 1 in 3 pts; 2 in 7 pts; 3 in 2 pts; 4 in 1 pt; 5 in 3 pts; 6 in 2 pts; 7 in 1 pt; and 11 in 1 pt). The clot volumes ranged from 0.0041–47.34 cm³ (mean +/- SD, 5.93 +/- 10.15 cm³). On the second read, analyst 1 found the same number and distribution of emboli. The clot volume range varied on the upper extent as compared to the initial read. The clot volumes for read 2

ranged from 0.0041-45.52 cm³ (mean +/- SD, 5.42 +/- 9.53 cm³).

Analyst 2 found 73 emboli in the 23 patients with a mean number of emboli of 3.17 per patient. With the three negative cases excluded the mean number of emboli per patient was 3.65. There was a range of 0-11 emboli per patient. (0 in 3 pts; 1 in 3 pts; 2 in 7 pts; 3 in 2 pts; 4 in 1 pt; 5 in 2 pts; 6 in 3 pts; 7 in 1 pt; and 11 in 1 pt). The clot volumes ranged from 0.00459-46.29 cm³ (mean +/- SD, 5.91 +/- 10.06cm³).

The ICC calculated for the TTV measurements per patient for inter-observer analysis was 0.998 and for intra-observer analysis was 0.997, while the associated Bland-Altman analyses for inter-and intra-observer agreement for TTV demonstrated no inter- or intra-observer biases (*P* = 0.23 for inter-observer results, *P* = 0.26 for intra-observer results for TTV using a one-sample *t*-test with 0, two tailed). The ICC and Bland-Altman analyses are seen in Figure 3. The ICC calculated for the ITV measurements per patient for inter-observer analysis was 0.996 and for intra-observer analysis was 0.997, while the associated Bland-Altman analyses for inter-and intra-observer agreement for ITV demonstrated no inter- or intra-observer biases. (*P* = 0.55 for inter-observer results, *P* = 0.24 for intra-observer results for TTV using a one-sample *t*-test with 0,

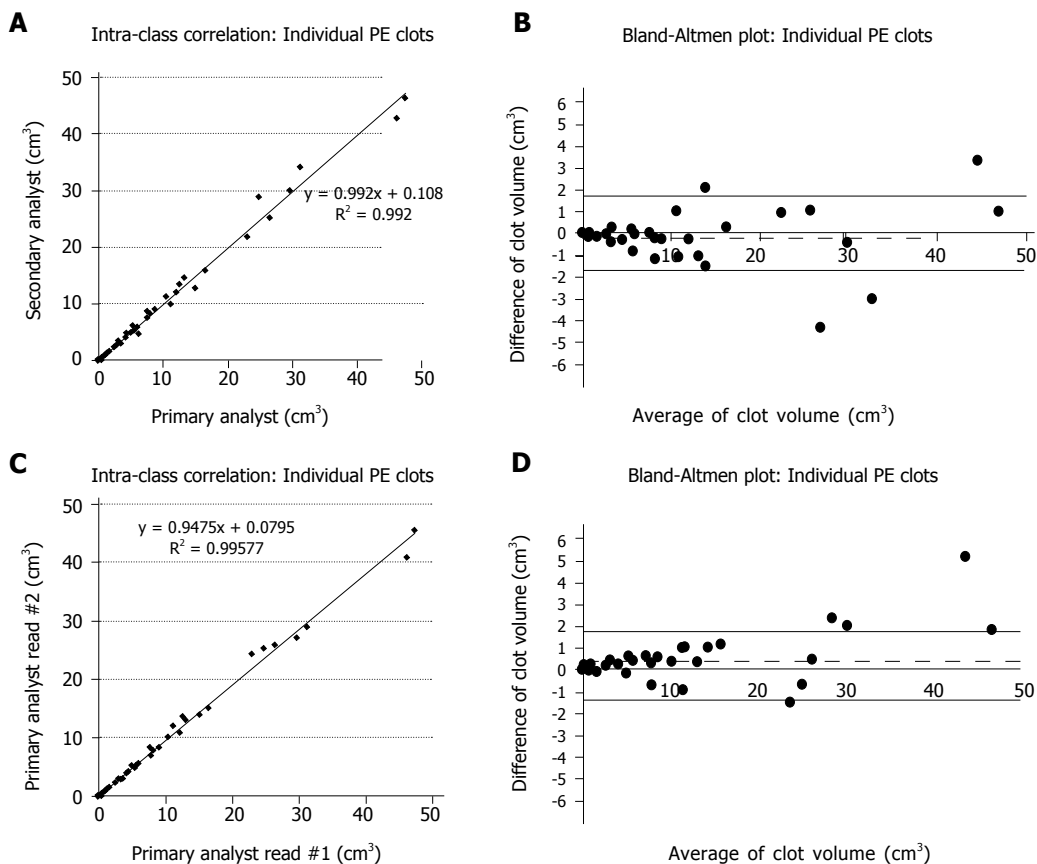


Figure 4 Individual thrombus volume inter- and intra-observer reproducibility (A) Intra-class correlation coefficient (ICC) plot and (B) Bland Altman plot comparing the individual PE thrombus volumes results of the primary and secondary image analyst for the inter-observer reproducibility analysis (C) ICC plot and (D) Bland Altman plot comparing the individual pulmonary embolism thrombus volumes results of the first and second read of the primary image analyst for the intra-observer reproducibility analysis.

two tailed). The ICC and Bland-Altman analyses for the ITV are seen in Figure 4.

A Qanadli score was calculated for each patient. The range of for Analyst 1 was 0%-52.5% for read one and 0%-52.5% for read two. The range for Analyst 2 was 0%-72.5%. The 20 positive cases had a mean Qanadli score with associated standard deviations of 37.25% +/- 16.93 and 39.125% +/- 19.20 for Analysts 1 and 2 respectively. The mean and standard deviation for Analyst 1's second read was 37.25% +/- 16.93. The ICC calculated for the Qanadli score per patient for inter- and intra-observer was 0.944 and 1 respectively. ICC plots and Bland Altman plots for inter- and intra-observer reproducibility for Qanadli assessment are shown in Figure 5.

The Modified Qanadli score was calculated for each patient as a secondary study endpoint. The range for Analyst 1 was 0%-70% for read one and 0%-72.5% for read two. The range of scores for Analyst 2 is 0%-72.5%. The 20 positive cases had a mean and associated standard deviations of 38.125% +/- 20.87 and 36.625% +/- 21.11 for Analysts 1 and 2 respectively. The mean and standard deviation for Analyst 1's second read was 38.5% +/- 21.34. The ICC calculated for the Modified Qanadli score per patient for inter- and intra-observer

was 0.996 and 0.999 respectively. ICC plots and Bland Altman plots for inter- and intra-observer reproducibility for the Modified Qanadli assessment are shown in Figure 6.

Finally, we also evaluated the % difference in TTV between the two analysts ($P = 0.074$, one sample t -test with zero, two tailed) as well as the two reads by Analyst 1 ($P = 0.063$, one sample t -test with 0, two tailed). These Bland-Altman plots are shown in Figure 7.

DISCUSSION

Emboli to the lungs cause physical obstruction of the pulmonary arteries yielding a pathophysiologic cascade resulting in varying degrees of cardiovascular distress^[19]. Although the embolic load and distribution are considered less pertinent than the patient's hemodynamic status in evaluating risk stratification^[7] clot burden has been shown to have predictive value of mortality in patients with acute PE^[20]. For example, Collomb *et al*^[21] have shown that the hemodynamic severity of acute PE can be determined by assessing clot burden through the use of a vascular obstruction index as well as other vascular load measurements such as right ventricular (RV): left ventricular (LV) ratio, minimum LV diameter

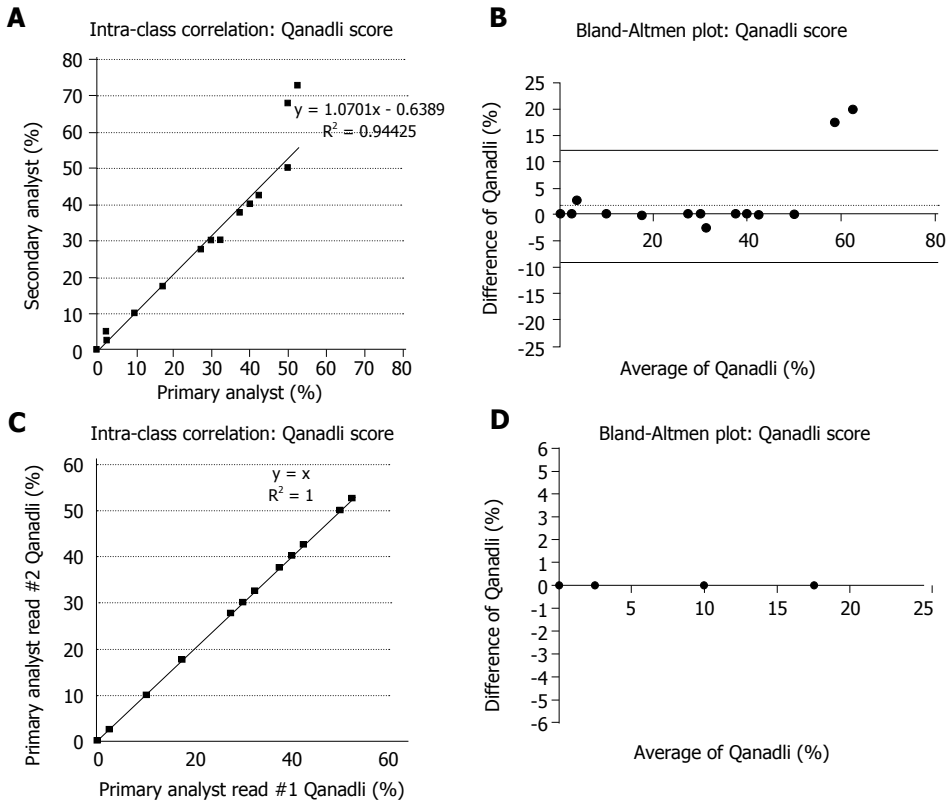


Figure 5 Qanadli score inter- and intra-observer reproducibility (A) Intra-class correlation coefficient (ICC) plot and (B) Bland Altman plot comparing the Qanadli score results of the primary and secondary image analyst for the inter-observer reproducibility analysis (C) ICC plot and (D) Bland Altman plot comparing the results of the first and second read of the primary image analyst for the intra-observer reproducibility analysis of the PE obstruction index (Qanadli score).

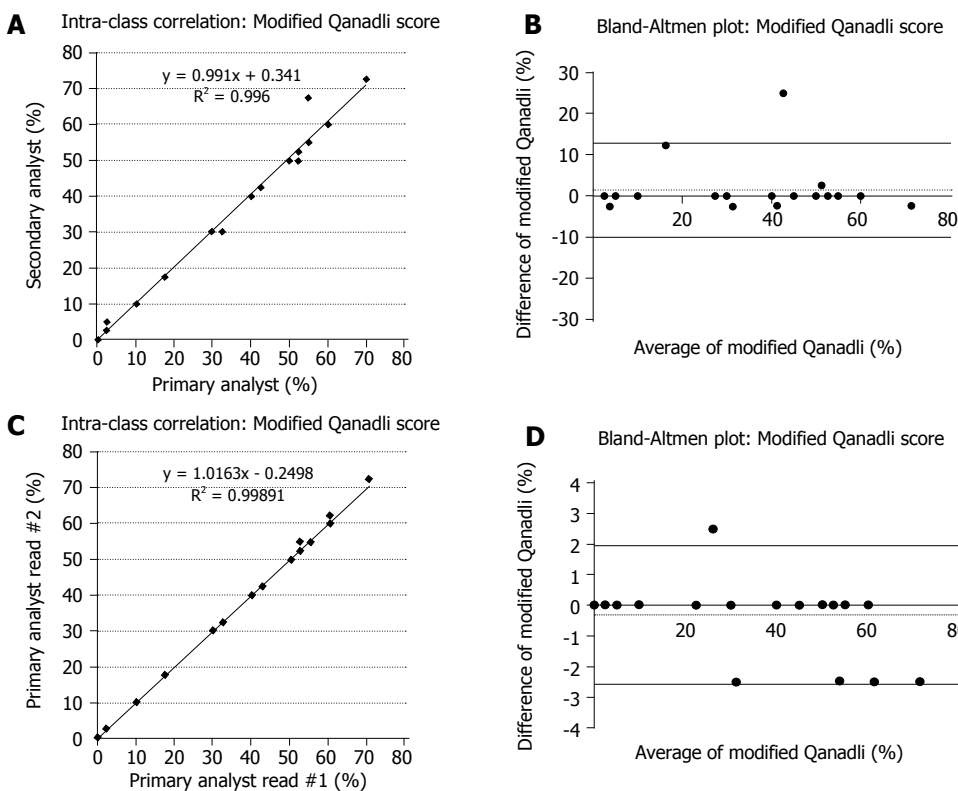


Figure 6 Modified Qanadli score inter- and intra-observer reproducibility (A) Intra-class correlation coefficient (ICC) plot and (B) Bland Altman plot comparing the modified Qanadli results of the primary and secondary image analyst for the inter-observer reproducibility analysis (C) ICC plot and (D) Bland Altman plot comparing the results of the first and second read of the primary image analyst for the intra-observer reproducibility analysis.

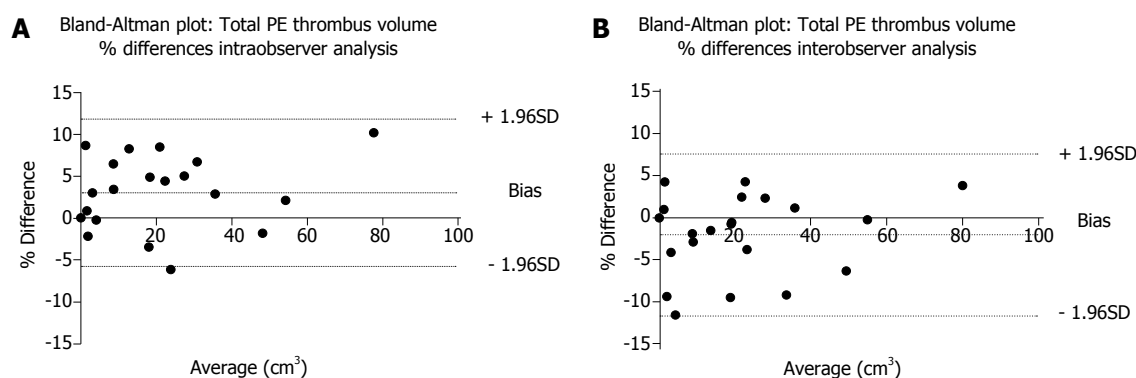


Figure 7 Bland Altman analysis of total thrombus volume normalized to clot size (Mean vs Difference/Mean) for (A) intra and (B) inter observer analysis.

and diameter of the central PA^[21]. Furthermore, Furlan *et al.*^[12] have shown that quantification of clot burden can be accurate and reproducible at a single institution. The challenges faced in multicenter studies include the variety of imaging systems and models used and the resultant variability in data acquisition. Additional variables could include differences in the energy level (kVp), pitch, reconstruction methods and contrast agents utilized.

Overall, inter- and intra-observer variability measurements indicated excellent reproducibility of the semi-automated analysis method for quantifying PE thrombus volume/burden. The ICC coefficient for all endpoints TTV (primary), ITV (secondary), Qanadli score (secondary) and modified Qanadli score (secondary) all had ICC values greater than 0.95 for both the inter- and intra-observer analysis. The Bland-Altman analysis also indicated no significant biases in any of the metrics evaluated. Our data showed that even with the variability inherent in multicenter data acquisition and reconstruction, the image analysis methodology employed here is reproducible and therefore suitable for use in a multicenter setting. These findings have implications on future studies of PE by allowing for both the option of multisite data acquisition with evaluation at an imaging core laboratory, as well as inclusion of direct PE volume measurements and assessment of temporal changes in embolic load. For example, in the SEATTLE II study, a multicenter investigation to assess the safety and efficacy of ultrasound-facilitated catheter-directed, low dose fibrinolysis therapy in patients with acute submassive PE, the RV/LV diameter ratio was used as a primary efficacy outcome^[22]. Subsequent research in SEATTLE II and similar studies can add direct clot burden volumetrics in furtherance of the body of knowledge in this area.

Our results compare well with those obtained by Nakada *et al.*^[23], who evaluated inter- and intra-reader reproducibility studies on manually measured PE volumes and showed no statistical differences in either inter- or intra-reader analyses. The intra-reader analysis in that study was nine months, much greater than in our study.

Implications of our findings on multicenter studies: In a recent study, we have shown that quantification

of clot volumes by CT is unaffected by most imaging acquisition and reconstruction parameters (except large differences in pitch used during acquisition)^[24]. Results of the current study show that the image analysis of data acquired from a multicenter setting is robust with the size of the clot not affecting the reproducibility of quantification significantly. Absolute quantification differences for TTV and ITV for both inter and intra-observer results were in the range of 2-4 cm³ (95%CI on Bland Altman plots, Figures 3 and 4). As a percent difference, these were of the order of 5%-10% (95%CI, Figure 7). This indicates that with our methodology we should be able to robustly pick up changes in absolute thrombus volume greater approximately 2 cm³ or 5% regardless of the starting size of the clots. This data can be used to estimate sample size requirements for clinical trials using clot burden quantification as an endpoint in PE treatment studies.

The study was limited by several factors. First, a small number of subjects were evaluated at a small number of sites. Images of subjects were chosen for this study during a site qualification visit prior to the start of a multicenter clinical trial evaluating a new thrombolytic agent for PE. Cases were also chosen to provide a spread of scanners and variations in imaging protocols across the sites. There could therefore be a selection bias in how these individuals were included as part of this current study. Second, the intra-reader variability analysis may have been affected by recall bias as there was a short interval of two weeks between the reads. This may have been insufficient to eliminate recall bias which could have resulted in the perfect agreement between the scores in the two reads. However, to reduce recall bias, images were presented to the image analyst in a randomized fashion for the two reads. Third, we were unable to assess radiation dose as a variable because the various scanners employ dose modulation and this setting is dependent upon patient size. Fourthly, we do not have access to demographic information of the subjects as the images analyzed were read anonymously and devoid of any Protected Health Information to comply with HIPAA requirements and our IRB approval. Fifthly, the inter reader assessments were only performed by 2 analysts and the intra reader

analysis was performed on two reads by only a single analyst. Analysis by more individuals will improve the robustness of the results. Lastly, Qanadli scoring may also be inherently skewed leading to high ICC because it relies on the weighting of affected proximal vascular branches thereby yielding specific discreet scores. This bias could be emphasized in our patient population that demonstrated large and often proximal PEs.

In conclusion, the data showed that our image analysis methodology is reproducible and therefore suitable for future use in a multicenter setting.

ARTICLE HIGHLIGHTS

Research background

In regard to clinical evaluation of pulmonary embolism (PE), clot burden is not a principal marker for clinical risk stratification, however clot burden is being used to assess for pharmaceutical characteristics in clinical drug trials in multicenter settings. To this point the technique has been studied with data obtained from a single imaging center using one fixed computed tomography pulmonary angiogram (CTPA) imaging protocol.

Research motivation

Data obtained from multicenter sites has not previously been studied. Thus, in order to validate the methods employed in multicenter clinical pharmaceutical trials of drugs such as thrombolytics, this study was commenced to assess for repeatability and consistency of clot volume measurements being obtained using semi-automated region growing techniques. Confirming the reliability of these measures has value in furthering the assessment of drug effectiveness, drug potency and in determination of optimal duration of therapy.

Research objectives

The key objective is to evaluate reproducibility of PE clot volume quantification using a semi-automated region growing algorithm on CTPA data in a multicenter setting.

Research methods

Anonymized CTPA data was acquired from 23 scanners from 18 imaging centers using each site's standard PE protocol. Two independent analysts measured PE volumes using a semi-automated region-growing algorithm on an FDA-approved image analysis platform. Total thrombus volume was calculated per patient as the primary endpoint. Secondary endpoints were individual thrombus volume, Qanadli score and modified Qanadli score per patient. Inter- and intra-observer reproducibility were assessed using intra-class correlation coefficient (ICC) and Bland-Altman analysis. The methods employed in this study were novel in that they previously have not been used in a multicenter setting.

Research results

The results showed excellent reproducibility of inter- and intra-observer variability measurements using the semi-automated region-growing method for quantifying PE volume burden. ICC for all endpoints was greater than 0.95 for inter- and intra-observer analysis. Bland-Altman analysis indicated no significant biases. The results confirm the validity of the methods used in multicenter pharmaceutical trials thereby allowing for advancement in this field.

Research conclusions

Semi-automated region growing algorithm for quantifying PE is reproducible using data from multiple scanners and is a suitable method for image analysis in multicenter clinical trials. The utility of validating this method could affect the advancement of thrombolytic therapy and other interventions that may be used to treat PE.

Research perspectives

Computer-assisted image analysis has a growing role in both diagnostic and investigative imaging. This study solidifies the foundation of semi-automated

region growing for volume quantification by proving the repeatability of the technique when used in a multicenter setting.

ACKNOWLEDGEMENTS

This study is supported by Daiichi Sankyo Pharma Development. In addition, we wish to acknowledge the following hospitals, site names, principal investigators, and radiologists. Dr. Saskia Middeldorp and Dr. Ludo Beenen - Academic Medical Center, Amsterdam, Netherlands; Dr. Aldo Salvi, Dr. Cinzia Nitti and Dr. Arianna Lorenzoni - Azienda Ospedaliero Universitaria Ospedali Riuniti Di Ancona, Ancona, Italy; Dr. Claudio Cuccia and Dr. Silvia Magnaldi - Fondazione Poliambulanza Istituto Ospedaliero, Brescia, Italy; Dr. Francis Couturaud and Dr. Michel Nonent - Hôpital de la Cavale Blanche, Brest, France; Dr. Franck Verschuren and Dr. Benoit Ghaye - Cliniques Universitaires Saint-Luc, Brussels, Belgium; Dr. Jeannot Schmidt and Dr. Lucie Cassagnes - CHU de Clermont-Ferrand, Clermont-Ferrand, France; Dr. Fernando Garcia-Bragado and Dr. Pedro Ortuno Muro - Hospital Universitario Dr. Josep Trueta, Girona, Spain; Dr. Marianne Brodmann and Dr. Reinhard Raggam - Medical University Graz, Graz, Austria; Dr. Klaus Empen and Dr. Birger Mensel - Universitätsmedizin Greifswald, Greifswald, Germany; Dr. Helen Bouvaist and Dr. Adrien Jankowski - Hopital Michallon - CHUGA, Grenoble, France; Dr. Menno Huisman and Dr. Lucia Kroft - Leiden University Medical Center, Leiden, Netherlands; Dr. Peter Verhammo, Dr. Johny Verschakelen and Dr. Walter Coudyzer - UZ Gasthuisberg, Leuven, Belgium; Dr. Victor Tapson and Dr. Peter Julien - Cedars Sinai Medical Center, Los Angeles, United States; Dr. David Jimenez and Dr. Agustina Vicente Bartulos - Hospital Universitario Ramon y Cajal, Madrid, Spain; Dr. Maurizio Concha - Intercoastal Medical Group, Sarasota, United States; Dr. Laurent Bertuletti and Dr. Pierre Croisille - CHU de St. Etienne, St. Etienne, France; Dr. Dominique Stephan and Dr. Michael Ohana - Strasbourg University Hospital, Strasbourg, France and Dr. Walter Ageno and Dr. Chiara Floridi - Ospedale di Circolo, University of Insubria, Varese, Italy.

REFERENCES

- 1 **Wakefield TW**, McLafferty RB, Lohr JM, Caprini JA, Gillespie DL, Passman MA; Executive Committee of the American Venous Forum. Call to action to prevent venous thromboembolism. *J Vasc Surg* 2009; **49**: 1620-1623 [PMID: 19497526 DOI: 10.1016/j.jvs.2009.01.058]
- 2 **Heit JA**. Venous thromboembolism: disease burden, outcomes and risk factors. *J Thromb Haemost* 2005; **3**: 1611-1617 [PMID: 16102026 DOI: 10.1111/j.1538-7836.2005.01415.x]
- 3 **Silverstein MD**, Heit JA, Mohr DN, Petterson TM, O'Fallon WM, Melton LJ 3rd. Trends in the incidence of deep vein thrombosis and pulmonary embolism: a 25-year population-based study. *Arch Intern Med* 1998; **158**: 585-593 [PMID: 9521222 DOI: 10.1001/archinte.158.6.585]
- 4 **Heit JA**, Silverstein MD, Mohr DN, Petterson TM, O'Fallon WM, Melton LJ 3rd. Predictors of survival after deep vein thrombosis and pulmonary embolism: a population-based, cohort study. *Arch Intern Med* 1999; **159**: 445-453 [PMID: 10074952 DOI: 10.1001/archinte.159.5.445]
- 5 **Laporte S**, Mismetti P, Décousus H, Uresandi F, Otero R,

- Lobo JL, Monreal M; RIETE Investigators. Clinical predictors for fatal pulmonary embolism in 15,520 patients with venous thromboembolism: findings from the Registro Informatizado de la Enfermedad TromboEmbolica venosa (RIETE) Registry. *Circulation* 2008; **117**: 1711-1716 [PMID: 18347212 DOI: 10.1161/CIRCULATIONAHA.107.726232]
- 6 **Goldhaber SZ**, Visani L, De Rosa M. Acute pulmonary embolism: clinical outcomes in the International Cooperative Pulmonary Embolism Registry (ICOPER) *Lancet* 1999; **353**: 1386-1389 [PMID: 10227218 DOI: 10.1016/S0140-6736(98)07534-5]
 - 7 **Tapson VF**. Diagnosis, prognosis and therapeutic management of acute pulmonary embolism. *Hosp Pract* (1995) 2016; **44**: 164-172 [PMID: 27450108 DOI: 10.1080/21548331.2016.1210471]
 - 8 **Torbicki A**, Perrier A, Konstantinides S, Agnelli G, Galiè N, Pruszczyk P, Bengel F, Brady AJ, Ferreira D, Janssens U, Klepetko W, Mayer E, Remy-Jardin M, Bassand JP; ESC Committee for Practice Guidelines (CPG). Guidelines on the diagnosis and management of acute pulmonary embolism: the Task Force for the Diagnosis and Management of Acute Pulmonary Embolism of the European Society of Cardiology (ESC). *Eur Heart J* 2008; **29**: 2276-2315 [PMID: 18757870 DOI: 10.1093/eurheartj/ehn310]
 - 9 **Hariharan P**, Dudzinski DM, Rosovsky R, Haddad F, MacMahon P, Parry B, Chang Y, Kabrhel C. Relation Among Clot Burden, Right-Sided Heart Strain, and Adverse Events After Acute Pulmonary Embolism. *Am J Cardiol* 2016; **118**: 1568-1573 [PMID: 27742425 DOI: 10.1016/j.amjcard.2016.08.025]
 - 10 **Meinel FG**, Nance JW Jr, Schoepf UJ, Hoffmann VS, Thierfelder KM, Costello P, Goldhaber SZ, Bamberg F. Predictive Value of Computed Tomography in Acute Pulmonary Embolism: Systematic Review and Meta-analysis. *Am J Med* 2015; **128**: 747-59.e2 [PMID: 25680885 DOI: 10.1016/j.amjmed.2015.01.023]
 - 11 **Vedovati MC**, Becattini C, Agnelli G, Kamphuisen PW, Masotti L, Pruszczyk P, Casazza F, Salvi A, Grifoni S, Carugati A, Konstantinides S, Schreuder M, Golebiowski M, Duranti M. Multidetector CT scan for acute pulmonary embolism: embolic burden and clinical outcome. *Chest* 2012; **142**: 1417-1424 [PMID: 22628491 DOI: 10.1378/chest.11-2739]
 - 12 **Furlan A**, Patil A, Park B, Chang CC, Roberts MS, Bae KT. Accuracy and reproducibility of blood clot burden quantification with pulmonary CT angiography. *AJR Am J Roentgenol* 2011; **196**: 516-523 [PMID: 21343492 DOI: 10.2214/AJR.10.4603]
 - 13 **Aghayev A**, Furlan A, Patil A, Gumus S, Jeon KN, Park B, Bae KT. The rate of resolution of clot burden measured by pulmonary CT angiography in patients with acute pulmonary embolism. *AJR Am J Roentgenol* 2013; **200**: 791-797 [PMID: 23521450 DOI: 10.2214/AJR.12.8624]
 - 14 **Adams R**, Bischof L. Seeded region growing. *IEEE Trans Pattern Anal Mach Intell* 1994; **16**: 641-647 [DOI: 10.1109/34.295913]
 - 15 **Boser BE**, Guyon IM, Vapnik VN. A training algorithm for optimal margin classifiers. Proc. fifth Annu. Work. Comput. *ACM Press* 1992; 144-152 [DOI: 10.1145/130385.130401]
 - 16 **Malik J**, Belongie S, Leung T, Shi J. Contour and Texture Analysis for Image Segmentation. *Int J Comput Vis* 2001; **43**: 7-27 [DOI: 10.1023/A:1011174803800]
 - 17 **Qanadli SD**, El Hajjam M, Vieillard-Baron A, Joseph T, Mesurrolle B, Oliva VL, Barré O, Bruckert F, Dubourg O, Lacombe P. New CT index to quantify arterial obstruction in pulmonary embolism: comparison with angiographic index and echocardiography. *AJR Am J Roentgenol* 2001; **176**: 1415-1420 [PMID: 11373204 DOI: 10.2214/ajr.176.6.1761415]
 - 18 **Obradović D**, Joveš B, Pena Karan S, Stefanović S, Ivanov I, Vukoja M. Correlation between the Wells score and the Qanadli index in patients with pulmonary embolism. *Clin Respir J* 2016; **10**: 784-790 [PMID: 25763885 DOI: 10.1111/crj.12291]
 - 19 **Piazza G**, Goldhaber SZ. Management of submassive pulmonary embolism. *Circulation* 2010; **122**: 1124-1129 [PMID: 20837937 DOI: 10.1161/CIRCULATIONAHA.110.961136]
 - 20 **El-Menyar A**, Nabir S, Ahmed N, Asim M, Jabbour G, Al-Thani H. Diagnostic implications of computed tomography pulmonary angiography in patients with pulmonary embolism. *Ann Thorac Med* 2016; **11**: 269-276 [PMID: 27803753 DOI: 10.4103/1817-1737.191868]
 - 21 **Collomb D**, Paramelle PJ, Calaque O, Bosson JL, Vanzetto G, Barnoud D, Pison C, Coulomb M, Ferretti G. Severity assessment of acute pulmonary embolism: evaluation using helical CT. *Eur Radiol* 2003; **13**: 1508-1514 [PMID: 12835961 DOI: 10.1007/s00330-002-1804-5]
 - 22 **Piazza G**, Hohlfelder B, Jaff MR, Ouriel K, Engelhardt TC, Sterling KM, Jones NJ, Gurley JC, Bhatheja R, Kennedy RJ, Goswami N, Natarajan K, Rundback J, Sadiq IR, Liu SK, Bhalla N, Raja ML, Weinstock BS, Cynamon J, Elmasri FF, Garcia MJ, Kumar M, Ayerdi J, Soukas P, Kuo W, Liu PY, Goldhaber SZ; SEATTLE II Investigators. A Prospective, Single-Arm, Multicenter Trial of Ultrasound-Facilitated, Catheter-Directed, Low-Dose Fibrinolysis for Acute Massive and Submassive Pulmonary Embolism: The SEATTLE II Study. *JACC Cardiovasc Interv* 2015; **8**: 1382-1392 [PMID: 26315743 DOI: 10.1016/j.jcin.2015.04.020]
 - 23 **Nakada K**, Okada T, Osada H, Honda N. Relation between pulmonary embolus volume quantified by multidetector computed tomography and clinical status and outcome for patients with acute pulmonary embolism. *Jpn J Radiol* 2010; **28**: 34-42 [PMID: 20112091 DOI: 10.1007/s11604-009-0380-x]
 - 24 **Kaufman AE**, Pruzan AN, Hsu C, Ramachandran S, Jacobi A, Fayad ZA, Mani V. Effect of varying computed tomography acquisition and reconstruction parameters on semi-automated clot volume quantification. *World J Radiol* 2018; **10**: 24-29 [PMID: 29599936 DOI: 10.4329/wjr.v10.i3.24]

P- Reviewer: Bazeed MF, Bazeed J, Gao BL, Kwok WE, Valek V

S- Editor: Cui LJ **L- Editor:** A **E- Editor:** Wu YXJ



Observational Study

Low-radiation and high image quality coronary computed tomography angiography in “real-world” unselected patients

Caryl Elizabeth Richards, Stephen Dorman, Patricia John, Anthony Davies, Sharon Evans, Tishi Ninan, David Martin, Sriranj Kannoly, Gail Roberts-Davies, Mark Ramsey, Daniel Rhys Obaid

Caryl Elizabeth Richards, Daniel Rhys Obaid, Swansea University Medical School, Swansea University, Grove Building, Singleton Park, Sketty, Swansea SA2 8PP, United Kingdom

Stephen Dorman, Mark Ramsey, Daniel Rhys Obaid, Department of Cardiology, Morriston Hospital, Heol Maes Eglwys, Morriston, Cwmrhydyceirw, Swansea SA6 6NL, United Kingdom

Patricia John, Anthony Davies, Sharon Evans, Tishi Ninan, Department of Radiology, Morriston Hospital, Heol Maes Eglwys, Morriston, Cwmrhydyceirw, Swansea SA6 6NL, United Kingdom

David Martin, Gail Roberts-Davies, Department of Radiology, Singleton Hospital, Sketty Ln, Sketty, Swansea SA2 8QA, United Kingdom

Sriranj Kannoly, Department of Cardiology, Singleton Hospital, Sketty Ln, Sketty, Swansea SA2 8QA, United Kingdom

ORCID number: Caryl Elizabeth Richards (0000-0002-1044-1825); Stephen Dorman (0000-0003-3264-521X); Patricia John (0000-0002-7250-9995); Anthony Davies (0000-0002-4445-6427); Sharon Evans (0000-0001-9206-1051); Tishi Ninan (0000-0001-6547-6921); David Martin (0000-0002-1185-0196); Sriranj Kannoly (0000-0002-6840-3899); Gail Roberts-Davies (0000-0002-7880-4450); Mark Ramsey (0000-0003-3912-6658); Daniel Rhys Obaid (0000-0002-3891-1403).

Author contributions: Obaid DR designed the study; all authors performed the research; Richards CE analyzed the data and wrote the paper; Obaid DR revised the manuscript for final submission.

Institutional review board statement: As the study involved no deviation from standard treatment protocols and no randomization it was not considered “research requires ethical approval” by the NHS Research authority tool.

Informed consent statement: As this study does not involve

patient randomization or any deviation from standard treatment protocols and as it was deemed “non - research” by the NHS Health Research Authority tool no informed consent forms were used

Conflict-of-interest statement: None of the authors have any conflicts of interest or financial disclosure related to this study.

Data sharing statement: No additional data are available.

STROBE Statement: The authors have read the STROBE Statement-checklist of items, and the manuscript was prepared and revised according to the STROBE Statement-checklist of items.

Open-Access: This article is an open-access article which was selected by an in-house editor and fully peer-reviewed by external reviewers. It is distributed in accordance with the Creative Commons Attribution Non Commercial (CC BY-NC 4.0) license, which permits others to distribute, remix, adapt, build upon this work non-commercially, and license their derivative works on different terms, provided the original work is properly cited and the use is non-commercial. See: <http://creativecommons.org/licenses/by-nc/4.0/>

Manuscript source: Invited manuscript

Correspondence to: Daniel Rhys Obaid, PhD, Associate Professor, Department of Cardiology, Morriston Hospital, Heol Maes Eglwys, Morriston, Cwmrhydyceirw, Swansea SA6 6NL, United Kingdom. daniel.obaid@wales.nhs.uk
Telephone: +44-1792-704123
Fax: +44-1792-704149

Received: April 30, 2018

Peer-review started: April 30, 2018

First decision: June 6, 2018

Revised: August 14, 2018

Accepted: October 8, 2018

Article in press: October 8, 2018

Published online: October 28, 2018

Abstract

AIM

To determine the radiation dose and image quality in coronary computed tomography angiography (CCTA) using state-of-the-art dose reduction methods in unselected "real world" patients.

METHODS

In this single-centre study, consecutive patients in sinus rhythm underwent CCTA for suspected coronary artery disease (CAD) using a 320-row detector CT scanner. All patients underwent the standard CT acquisition protocol at our institute (Morrison Hospital) a combination of dose saving advances including prospective electrocardiogram-gating, automated tube current modulation, tube voltage reduction, heart rate reduction, and the most recent novel adaptive iterative dose reconstruction 3D (AIDR3D) algorithm. The cohort comprised real-world patients for routine CCTA who were not selected on age, body mass index, or heart rate. Subjective image quality was graded on a 4-point scale (4 = excellent, 1 = non-diagnostic).

RESULTS

A total of 543 patients were included in the study with a mean body weight of 81 ± 18 kg and a pre-scan mean heart rate of 70 ± 11 beats per minute (bpm). When indicated, patients received rate-limiting medication with an oral beta-blocker followed by additional intravenous beta-blocker to achieve a heart rate below 65 bpm. The median effective radiation dose was 0.88 mSv (IQR, 0.6-1.4 mSv) derived from a Dose Length Product of 61.45 mGy.cm (IQR, 42.86-100.00 mGy.cm). This also includes what we believe to be the lowest ever-reported radiation dose for a routine clinical CCTA (0.18 mSv). The mean image quality (\pm SD) was 3.65 ± 0.61 , with a subjective image quality score of 3 ("good") or above for 93% of patient CCTAs.

CONCLUSION

Combining a low-dose scan protocol and AIDR3D with a 320-detector row CT scanner can provide high quality images at exceptionally low radiation dose in unselected patients being investigated for CAD.

Key words: Effective radiation dose; Tube voltage; Tube current; Iterative reconstruction; Coronary computed tomography angiography; Image quality; Prospectively electrocardiogram gating

© **The Author(s) 2018.** Published by Baishideng Publishing Group Inc. All rights reserved.

Core tip: Coronary computed tomography angiography (CCTA) is now widely used in the diagnosis of coronary artery disease since it is a rapid, minimally invasive test with high diagnostic accuracy. To meet the demands for increasing spatial and temporal resolution of CT images, a number of dose saving algorithms have been implemented to CCTA to minimise radiation exposure to "as low as reasonably achievable" without compromising

diagnostic image quality. This study demonstrates that advances in CT scanner hardware and reconstruction software allow ultra-low dose of radiation with high image quality in routine clinical examination of real-world patients.

Richards CE, Dorman S, John P, Davies A, Evans S, Ninan T, Martin D, Kannoly S, Roberts-Davies G, Ramsey M, Obaid DR. Low-radiation and high image quality coronary computed tomography angiography in "real-world" unselected patients. *World J Radiol* 2018; 10(10): 135-142 Available from: URL: <http://www.wjgnet.com/1949-8470/full/v10/i10/135.htm> DOI: <http://dx.doi.org/10.4329/wjr.v10.i10.135>

INTRODUCTION

Coronary computed tomography angiography (CCTA) is increasingly being used in the diagnosis of coronary artery disease (CAD) since it is rapid and minimally invasive^[1,2]. However, the high radiation doses^[3] previously required for optimising the image signal-to-noise ratio in CCTA were a major healthcare concern due to an associated increase in lifetime risk of radiation-induced malignancy^[4]. CCTA has thus been a driving force behind a number of dose reduction strategies to pursue radiation exposure to "as low as reasonably achievable" (ALARA) without compromising image quality^[5].

Sub-millisievert CCTA was initially proven feasible in 2009 using dual-source CT with prospectively electrocardiogram (ECG)-triggered high-pitch spiral acquisition^[6], and doses as low as 0.06 mSv have been reported using this technique with a combination of iterative reconstruction (IR) and reduced tube voltage^[7]. However, these were conducted on highly selected populations with low body weight and heart rate. We prospectively analyzed the radiation exposure and image quality in consecutive unselected patients undergoing CCTA for suspected coronary disease with a 320-detector row CT scanner and IR, and active reduction of tube voltage, exposure window, and volume coverage.

MATERIALS AND METHODS

Patient cohort

This is a prospective single-centre study of 549 consecutive patients (age >18 years) who were referred to our institute between June 2012 and August 2016 to undergo CCTA for suspected CAD. Patients were excluded if they were undergoing cardiac CT for other indications (*e.g.*, assessment for trans-catheter aortic valve replacement or atrial fibrillation ablation). Patients were not pre-selected according to age, heart rate or body mass index (BMI).

CT scanner parameters

All examinations were performed on a 320-slice CT scanner with 320 mm \times 0.5 mm detector rows giving

z-axis coverage of 160 mm (Aquilion One, Toshiba Medical Systems, Japan). After acquisition of scout images, prospective ECG-gated CCTA was performed using half-segment reconstruction and a 350 ms rotation time. Scanning field of view was selected based on scout images using volume sizes of 100-160 mm and radiographer led to be the smallest possible that included the area of clinical interest (20 mm below carina to base of heart). Iodinated contrast media-75 mL of Iohexol (Omnipaque 300 if BMI < 30 kg/m², (Omnipaque 350 if BMI > 30 kg/m²)-was injected in a biphasic protocol at 5 mL/s triggered by bolus tracking.

The Sure Cardio Prospective Package was used to reduce the exposure window depending on heart rate. For patients with a heart rate below 65 bpm, images were acquired with an acquisition window of 70%-80% of the interval between two consecutive QRS complexes. If patients had a heart rate below 60 bpm the acquisition window could be reduced further at the radiographer's discretion. Tube current and voltage were also minimised according to each patient's BMI and density, using the Sure Exposure 3D (SUREexposure, Toshiba Medical Systems, Japan) with an automatic exposure control system.

Unless contraindicated, patients received rate-limiting medication as required with an oral beta-blocker (atenolol 25 mg) followed by additional intravenous beta-blocker (metoprolol 5-25 mg) aiming for a heart rate below 65 bpm. All patients also received sublingual glyceryl trinitrate (300 µg).

The effective radiation dose for each patient was derived by multiplying the dose-length product (DLP), recorded from the CT scanner, by the conversion factor 0.014 mSv mGy⁻¹ cm⁻¹, according to guidelines from the International Commission on Radiological Protection^[8]. The effective radiation dose can then be compared to the lowest mean effective doses recorded in literature. In patients with repeated coronary CT angiography scans, the cumulative DLP and the cumulative effective dose were included in the analysis.

Image reconstruction and analysis

Images were reconstructed with a section thickness of 0.5 mm and an increment of 0.25 mm using the Adaptive Iterative Dose Reconstruction 3D (AIDR3D) algorithm. CCTA images were analyzed on a dedicated post-processing workstation by two trained observers. Subjective image quality was assessed by the two trained observers and scored on a four-point scale (4 = excellent, 1 = non-diagnostic). If any patients went on to undergo invasive coronary angiography then the accuracy of CCTA in determining the presence of significant coronary disease (stenosis > 50%) compared with the gold standard of invasive angiography was recorded.

RESULTS

CT data from a total of 543 consecutive patients who

underwent CCTA for suspected CAD were assessed. A total of six patients were excluded from the evaluation due to failure to perform CCTA; four patients due to an inability to obtain intravenous access and two patients from incomplete dose data.

Table 1 summarises the characteristics of the 543 patients included in the final analysis. The mean age was 56 ± 11 years; and 33% were male. The mean body weight was 81 ± 18 kg and mean heart rate was 70 ± 11 bpm. Additional IV metoprolol was required in 47% of the scans. The presence of CAD was confirmed by CCTA in 57 (10%) of patients.

Radiation dose

The median DLP for all 543 patients was 61.45 mGy.cm (IQR, 42.86-100.00 mGy.cm) corresponding to a median effective dose of 0.88 mSv (IQR, 0.6-1.4 mSv). A total of 23 scans were repeated and whose cumulative radiation doses were thus included in the final median dose value. The frequency of the per-patient radiation dose, plotted in Figure 1, indicates a high positive skew with a Pearson coefficient of 3.26 from the normal distribution. This further demonstrates that the majority of patients received a very low dose of radiation and those that received a high dose were few in number.

A total of 328 (56%) patients received an effective dose < 1 mSv, 409 patients (75%) received an effective dose < 1.5 mSv. Moreover, we believe we have demonstrated the lowest ever-recorded effective dose for a CCTA performed in routine clinical practice of 0.18 mSv with a subjective image quality score of 4 (Figure 2).

Image quality

The mean image quality (± SD) for all 543 scans was 3.65 ± 0.61 with a corresponding score breakdown; excellent 392 (72%), good 118 (22%), poor but usable 30 (5%), and poor 3 (1%). We compared the patient characteristics of the excellent and good scans (image quality score 3 + 4) with those that were poor and unusable (image quality score 1 + 2). There was no difference in mean age or sex between the groups. However, compared with excellent and good scans, poor and unusable scans were more likely to occur in patients with heart rates > 65 bpm (31% vs 9%, *P* < 0.0001) and require a higher effective dose (1.98 ± 1.69 vs 1.24 ± 1.41, *P* = 0.0041) (Table 2).

Twenty-one of the patients underwent invasive coronary angiography in addition to CCTA yielding 84 coronary arteries for comparison (21 left main stem, 21 left anterior descending, 21 left circumflex and 21 right coronary artery). CCTA correctly identified a significant (> 50%) stenosis in 16/17 coronary arteries and correctly excluded significant stenosis in 62/67 coronary arteries. This gave CCTA a sensitivity of 94%, specificity 93%, negative predictive value 98% and positive predictive value 76% to identify a significantly (> 50%) stenosis coronary artery in comparison with the gold standard of

Table 1 Patient characteristics

| Parameter | n (%) | |
|------------------------------|-----------------------|----------|
| Number of patients | 543 | |
| Age (yr) | 56 ± 11 | |
| Gender | Male/Female (33%/67%) | |
| Mean weight (kg) | 81 ± 18 ¹ | |
| Mean heart rate (bpm) | 70.3 ± 11.4 | |
| Oral Beta-blocker | 204 (38) | |
| IV Beta-blocker | 255 (47) | |
| Heart rate during scan (bpm) | < 60 bpm | 349 (64) |
| | 60-65 bpm | 112 (21) |
| | 65-75 bpm | 55 (10) |
| | > 75 bpm | 18 (3) |
| | Not recorded | 11 (2) |

¹Weight data only available for 32% of the patients.

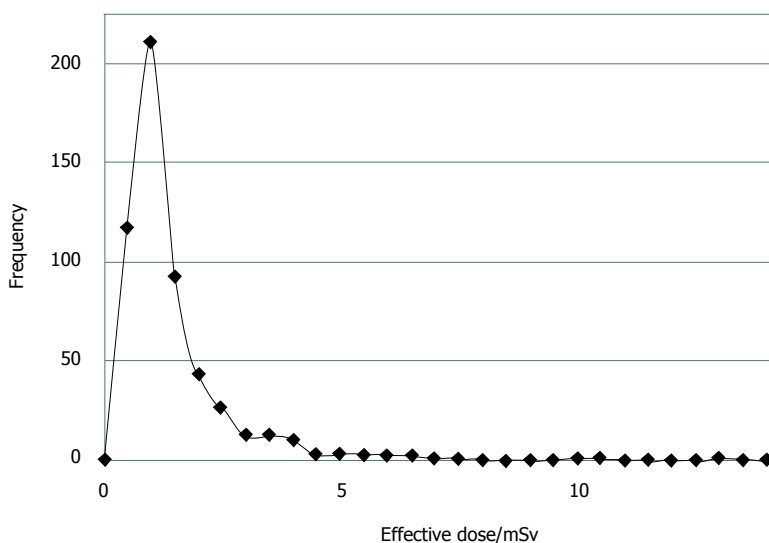


Figure 1 Distribution of effective doses for patients undergoing coronary computed tomography angiography.

invasive angiography. Examples of correct and incorrect CCTA classifications are provided in Figure 3.

DISCUSSION

We analyzed the CCTA data of 543 unselected consecutive patients with suspected CAD. The median effective radiation dose was 0.88 mSv (IQR, 0.6-1.4 mSv) with diagnostic image quality in 99% of patients, verifying that sub-millisievert radiation doses are possible in unselected, real-world patients undergoing CCTA.

A number of integrated strategies were used to achieve this consistently low dose, including; prospective ECG-gated acquisition, lowest possible tube current and voltage, IR (AIDR3D image reconstruction algorithm) and meticulous attention to patient preparation, both pre scan (heart rate control) and during the scan (reduction in volume of coverage to minimal size possible whilst allowing complete acquisition in a single volume.

Prospective ECG-gated tube current modulation is reported to be one of the most effective methods at redu-

cing the radiation dose. Unlike traditional retrospective-gating, where data are acquired over the whole heart phase, in prospective gating the X-ray tube is switched on only at predefined time-points of the cardiac cycle. In their systematic review, Menke *et al*^[9] confirmed a pooled effective dose of 3.5 mSv with prospective gating, a factor of 3.5 lower than the pooled effective dose of 12.3 mSv with retrospective gating.

Radiation dose increases with the square of the tube voltage at a constant tube current, reducing the tube voltage further lowers radiation exposure^[10]. Tube current and voltage were minimised to each patient’s BMI and density, using the Sure Exposure 3D (SUREExposure, Toshiba Medical Systems, Japan) with an automatic exposure control system which reduces tube current and voltage on the basis of scout images and the reconstruction kernel^[11].

However, dose reduction by lowering tube voltage and current causes a substantial increase in noise, especially in obese patients^[12]. To overcome these limitations and allow further dose reduction, new IR algorithms represent another milestone in CCTA^[13]. IR algorithms

Table 2 Characteristics of patients with image quality scores of 1 + 2 vs 3 + 4

| | Image quality score 1 + 2 | Image quality Score 3 + 4 | P value |
|--|---------------------------|---------------------------|------------|
| Female patient | 12/30 (63%) | 216/391 (67%) | P = 0.1068 |
| Mean age ± SD (years) | 57.5 ± 10.5 | 55.5 ± 10.6 | P = 0.2979 |
| No. of patients with heart rate ≤ 65 bpm | 22 (69%) | 457 (91%) | P < 0.0001 |
| No. of patients with heart rate > 65 bpm | 10 (31%) | 43 (9%) | P < 0.0001 |
| Effective dose ± SD (mSv) | 1.98 ± 1.69 | 1.24 ± 1.41 | P = 0.0041 |



Figure 2 Coronary computed tomography angiography examination with image quality score 4 performed in a 52 years old female patient with heart rate of 56 bpm with a dose of 0.18 mSv.

adaptively apply noise correction at a reduced X-ray exposure without compromising spatial resolution^[14]. AIDR and more recently 3D AIDR (AIDR3D) decreases image noise thus allowing for reductions in tube current while preserving overall image quality^[15]. BMI-adapted tube voltage and current work synergistically with AIDR3D to reduce image noise while achieving a 75% radiation dose reduction relative to a scan reconstructed with filtered back-projection^[16].

Patient irradiation is further limited by decreasing the craniocaudal field of view to the minimum required following analysis of the scout view^[17]. The wide area detector row CT scanner can be used with less than the maximum 16 cm (320-detector) craniocaudal coverage. For example, imaging over a 14 cm (280 detectors) craniocaudal field of view will decrease patient dose by 12.5% and is proven sufficient for most patients^[18].

The radiation dose with the 320-detector CT scanner is significantly lower if data acquisition occurs as a single volume^[19]. To facilitate this we were judicious in our use of beta-blockers to slow the resting heart rate. Lowering the heart rate with beta-blockers has previously shown to be a safe practice^[20], reducing radiation exposure and improving image quality^[21]. We achieved comparable X-ray doses in our real world population to Chen *et al.*^[19] using a 320-detector CT scanner despite a slower gantry rotation speed (350 ms vs 275 ms due to the aggressive measures to control heart rate, with 65% of

patients receiving betablockers [either oral only (15%), iv only (27%) or both (23%)] and 85% of patients achieving a heart rate < 65 bpm. Moreover, we have demonstrated what we believe is the lowest ever-recorded effective dose of 0.18 mSv with a subjective image quality score of 4 ("excellent") from a study of real-world unselected patients. This ultra-low radiation dose for CCTA is comparable to the radiation range reported for a chest X-ray in two views^[22]. Advances in radiation dose reduction without compromising image quality justify the use of CCTA as a non-invasive alternative to coronary catheterization in investigating appropriate populations for CAD^[23].

The prospective ECG-gated single volume acquisition with AIDR-3D protocol we use at our institution is not the only potential strategy for very low dose CCTA. Another contemporary strategy is Prospective ECG-triggered high-pitch spiral acquisition which also allows the entire heart to be scanned within one single cardiac cycle thus significantly lowering the radiation dose^[24-26]. This coupled with IR techniques have shown ultra-low mean effective radiation doses ranging from 0.06 mSv to 0.3 mSv with clinically acceptable diagnostic images^[7,27]. While demonstrating the feasibility of ultra-low dose CCTA, these studies were limited to carefully selected patients with a low and regular heart rate (< 60 bpm) and a body weight of less than 100 kg. Other IR algorithms are also in use including Model-based IR (MBIR, GE Healthcare, Waukesha, Wisconsin) which has also shown promising results for noise reduction in very-low-dose CCTA^[22]. iDose4 and iterative model reconstruction are alternative IR algorithms released by Philips Healthcare (Philips Healthcare, Best, the Netherlands) that have also maintained image quality at 80% lower radiation exposure^[13].

Our study has some limitations. Whilst we included all consecutive patients undergoing CCTA for the evaluation of suspected CAD we did not include cardiac CT performed for other indications such as evaluation of coronary bypass grafts, evaluation of left atrium anatomy prior to atrial fibrillation ablation, pre-operative assessment for trans-catheter aortic valve replacement or assessment of cardiac function so the same low doses may not be achieved in these patient groups. In addition, patients in atrial fibrillation were not included and whilst the patients were not selected on the basis

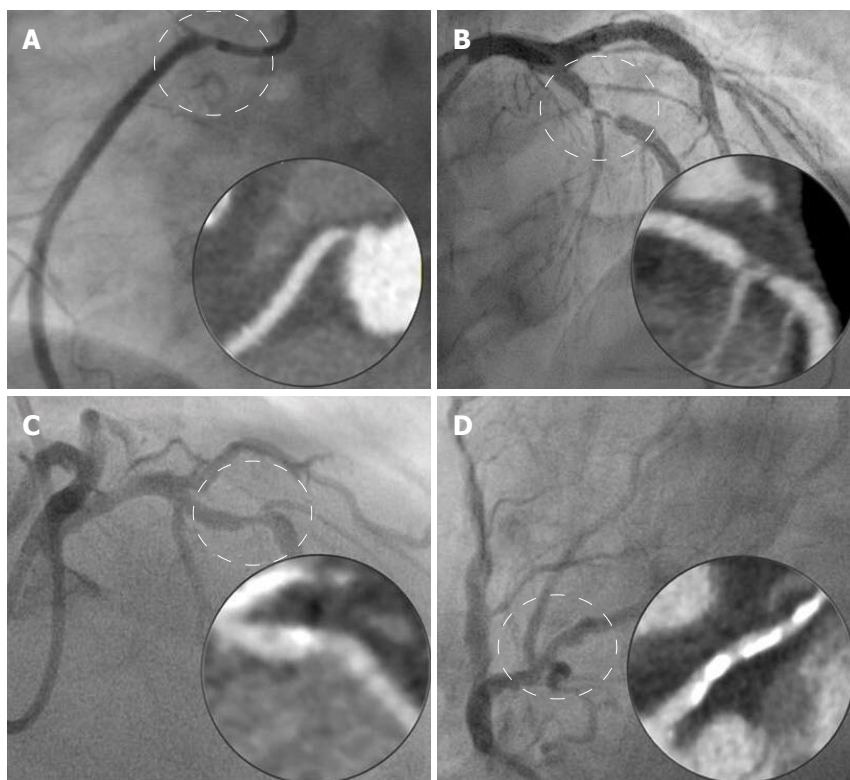


Figure 3 Examples of correlation of coronary computed tomography angiography with invasive angiography. A: Correct identification of ostial stenosis in right coronary; B: Correct identification of significant stenosis in left anterior descending coronary; C: Coronary computed tomography angiography (CCTA) incorrectly classifies lesion as not significant (subsequently proven to be haemodynamically significant with fractional flow reserve); D: CCTA incorrectly identifies a significant lesion in circumflex coronary due to artefact from extensive calcification.

of body weight, body mass index was not recorded and actual weight measurements were only available for 32% of the patients meaning the effect of patient weight on dose could not be investigated in this study. In view of this, the results may not be generalizable to patients who are overweight or in atrial fibrillation.

The image quality score used is a subjective assessment and was performed by the authors. Whilst the results of patients who underwent invasive coronary angiography are included, the proportion is relatively small and a more robust assessment of image adequacy would have been obtained if all patients had undergone the gold standard of invasive angiography.

Finally, the conversion factor to determine effective radiation dose equivalents has been a point of controversy^[28]. Previous ICRP conversion factors for the chest have varied from 0.012-0.026 mSv mGy⁻¹ cm⁻¹ potentially yielding even lower radiation estimates^[29].

CONCLUSION

We report a series of over 500 CCTAs performed at our health board with excellent image quality and median effective dose of 0.88 mSv. This includes the lowest ever-reported radiation dose for a routine clinical CCTA (0.18 mSv). We have demonstrated that provided patients are in sinus rhythm and with the judicious use of beta blockers to achieve heart rates < 65 bpm a

combination of low-dose CCTA scan protocol and AID-R3D with a 320-detector row CT scanner can provide high quality images at exceptionally low radiation dose in patients being investigated for CAD.

ARTICLE HIGHLIGHTS

Research background

Traditionally, coronary angiography has been the gold standard in diagnosing coronary artery disease (CAD). Coronary computed tomography angiography (CCTA), however, is increasingly being used as a rapid and less invasive alternative in diagnosing patients at risk of CAD. A 3D image of the heart and coronary circulation can be rendered with a CT scanner using only an intravenous injection of iodine-rich contrast, thus circumventing the need for insertion of a catheter via an artery or vein. However, imaging coronary arteries presents increased challenges, since it requires both a high temporal resolution to reduce motion artifacts caused by cardiac motion and a high spatial resolution to differentiate small coronary structures. While images obtained with CCTA scanners are now comparable to coronary angiography these CT requirements have previously resulted in higher radiation doses thus increasing the lifetime risk of radiation-induced malignancy. Advances in CCTA scanner hardware and image reconstruction techniques have led to reports of exceptionally low radiation doses, down to 0.06 mSv, while maintaining diagnostic image quality of the coronary arteries. For example, in prospective electrocardiogram-gated acquisition the X-ray tube is switched on only for a reduced percentage of the cardiac cycle rather than the whole cycle. Automatic exposure control uses the lowest possible CT tube current and voltage adjusted to the patient's body habitus. This works in synergy with novel image IR algorithms that adaptively apply noise correction to offset an increase in image noise caused by a reduced tube voltage. Using pharmacological methods to reduce heart rate, with oral or intravenous beta-blockers, has proven to reduce cardiac motion during the acquisition leading to improved images. An initial

scout view of the thorax can also be used to minimize the volume covered per-patient in a single complete acquisition to further reduce the radiation. However, these previous studies were conducted on small cohorts that were pre-selected for low body weight and heart rate, and were limited by a low prevalence of CAD. The feasibility and effect of these low-dose scan modes on both image quality and radiation exposure in a large patient population with various heart rates is currently unknown. In this study, we determined the radiation dose and subjective image quality using a combination of state-of-the-art CCTA acquisition protocols at our institution in consecutive unselected patients undergoing CCTA for suspected coronary disease.

Research motivation

Ultra-low radiation doses of less than one mSv have been reported in other feasibility studies. While these advances in cardiac CT may effectively lower radiation dose, these studies are limited to small cohorts of pre-selected patients with very low and regular heart rates and low body habitus and are thus not representative of the typical population undergoing screening for CAD. This study aims to determine the feasibility of these low-dose CCTA acquisition protocols adopted at our institution in an unselected cohort from a series of consecutive patients who underwent CCTA for suspected CAD. We hope that the outcome may demonstrate that CCTA is a viable, non-invasive alternative to coronary catheterization for screening low-risk populations with suspected CAD.

Research objectives

The primary end points of the study were effective radiation dose and image quality in patients not selected in term of heart rate and body habitus undergoing routine CCTA. Our objective was to demonstrate that low radiation doses were feasible for the majority of real-world patients undergoing routine screening for CAD with CCTA without losing diagnostic image quality.

Research methods

The radiation dose and subjective image quality were analysed over a total of 543 consecutive patients in sinus rhythm who underwent CCTA at our institute for suspected CAD between June 2012 and August 2016. Subjective image quality was assessed by the two trained observers and scored on a four-point scale (4 = excellent, 1 = non-diagnostic). Images were acquired with a 320-row detector CT scanner (Aquilion One, Toshiba Medical Systems, Japan) and a number of integrated packages that have been developed to reduce the radiation dose to as low as reasonably achievable. Prospective electrocardiogram (ECG)-gated acquisition was implemented using the SURE Cardio Prospective Package over an acquisition window of 70%–80% of the interval between two consecutive QRS complexes in patients with a heart rate below 65 bpm. The Sure Exposure 3D package (SURExposure, Toshiba Medical Systems, Japan) automatically adjusted to the lowest possible tube current and voltage in accordance with each patient's attenuation profile while noise reduction during each acquisition was implemented with the three-dimensional adaptive iterative dose reduction (AIDR-3D) image reconstruction algorithm. If necessary, patients were prepared prior to the scan with rate-limiting oral beta-blockers followed by additional intravenous beta-blocker to achieve a heart rate below 65 bpm unless contraindicated. During the scan, the volume of coverage was reduced to minimal size whilst allowing complete acquisition in a single volume. Contrary to previous studies in which the patients were prospectively selected, the patients were not selected based on age, heart rate, and body mass index. We believe that this is a better representation of real world patients who would be undergoing routine CCTA for diagnosis of CAD.

Research results

The median effective radiation dose was 0.88 mSv, which includes what we believe to be the lowest ever-reported radiation dose for a routine clinical CCTA (0.18 mSv). The mean image quality (\pm SD) was 3.65 ± 0.61 , with a subjective image quality score of 3 ("good") or above for 93% of patient CCTAs. CAD was confirmed by CCTA in 57 (10%) of patients.

Research conclusions

The median effective radiation dose was 0.88 mSv (IQR, 0.6–1.4 mSv) with a mean subjective image quality score (\pm SD) of 3.65 ± 0.61 averaged over 500

real-world unselected patients undergoing routine clinical CCTA. This ultra-low radiation dose for CCTA is comparable to the radiation range reported for a chest X-ray in two views. The data also includes what we believe to be the lowest ever-reported radiation dose for a routine clinical CCTA 0.18 mSv with a subjective image quality score of 4 ("excellent"). This demonstrates that low radiation dose CCTA can be used as a routine clinical screening tool for CAD without loss of diagnostic image quality. To date, radiation dose reduction advances in CCTA technology have only been reported in feasibility studies on small cohorts of highly selected patients with low body habitus and heart rate. This study demonstrates that low radiation CCTA with good image quality is possible for most patients undergoing routine screening for CAD with CCTA using a combination of commercially available, state-of-the-art cardiac CT technology advances. CCTA is rapid and non-invasive compared with coronary angiography and has reduced patient recovery time. The reduced risk in radiation-induced malignancy implies that CCTA is a feasible alternative to coronary angiography as a primary screening tool for patients with low risk CAD.

Research perspectives

This study did not include patients with atrial fibrillation or other cardiac CT indications such as evaluation of coronary bypass grafts, evaluation of left atrium anatomy prior to atrial fibrillation ablation, pre-operative assessment for trans-catheter aortic valve replacement or assessment of cardiac function. Feasibility studies with alternative dose-saving strategies have also recorded ultra-low mean effective radiation doses ranging from 0.06 mSv to 0.3 mSv with clinically acceptable diagnostic images. These include techniques such as prospective ECG-triggered high-pitch spiral acquisition but again were limited to carefully selected patients. Extending these techniques to unselected patients could highlight the need for alternative protocols for undertaking routine CCTA for assessment of different patient groups or to incorporate existing technology at other institutions.

REFERENCES

- 1 **Salavati A**, Radmanesh F, Heidari K, Dwamena BA, Kelly AM, Cronin P. Dual-source computed tomography angiography for diagnosis and assessment of coronary artery disease: systematic review and meta-analysis. *J Cardiovasc Comput Tomogr* 2012; **6**: 78-90 [PMID: 22226727 DOI: 10.1016/j.jcct.2011.10.018]
- 2 **Haberl R**, Tittus J, Böhme E, Czernik A, Richartz BM, Buck J, Steinbigler P. Multislice spiral computed tomographic angiography of coronary arteries in patients with suspected coronary artery disease: an effective filter before catheter angiography? *Am Heart J* 2005; **149**: 1112-1119 [PMID: 15976796 DOI: 10.1016/j.ahj.2005.02.048]
- 3 **Hausleiter J**, Meyer T, Hermann F, Hadamitzky M, Krebs M, Gerber TC, McCollough C, Martinoff S, Kastrati A, Schömig A, Achenbach S. Estimated radiation dose associated with cardiac CT angiography. *JAMA* 2009; **301**: 500-507 [PMID: 19190314 DOI: 10.1001/jama.2009.54]
- 4 **Einstein AJ**, Henzlova MJ, Rajagopalan S. Estimating risk of cancer associated with radiation exposure from 64-slice computed tomography coronary angiography. *JAMA* 2007; **298**: 317-323 [PMID: 17635892 DOI: 10.1001/jama.298.3.317]
- 5 **Halliburton SS**, Abbara S, Chen MY, Gentry R, Mahesh M, Raff GL, Shaw LJ, Hausleiter J; Society of Cardiovascular Computed Tomography. SCCT guidelines on radiation dose and dose-optimization strategies in cardiovascular CT. *J Cardiovasc Comput Tomogr* 2011; **5**: 198-224 [PMID: 21723512 DOI: 10.1016/j.jcct.2011.06.001]
- 6 **Lell M**, Marwan M, Schepis T, Pflöderer T, Anders K, Flohr T, Allmendinger T, Kalender W, Ertel D, Thierfelder C, Kuettner A, Ropers D, Daniel WG, Achenbach S. Prospectively ECG-triggered high-pitch spiral acquisition for coronary CT angiography using dual source CT: technique and initial experience. *Eur Radiol* 2009; **19**: 2576-2583 [PMID: 19760421 DOI: 10.1007/s00330-009-1558-4]
- 7 **Schuhbaeck A**, Achenbach S, Layritz C, Eisentopf J, Hecker F, Pflöderer T, Gauss S, Rixe J, Kalender W, Daniel WG, Lell M, Ropers D. Image quality of ultra-low radiation exposure coronary CT angiography with an effective dose < 0.1 mSv using high-

- pitch spiral acquisition and raw data-based iterative reconstruction. *Eur Radiol* 2013; **23**: 597-606 [PMID: 22983283 DOI: 10.1007/s00330-012-2656-2]
- 8 **Kalender WA**, Schmidt B, Zankl M, Schmidt M. A PC program for estimating organ dose and effective dose values in computed tomography. *Eur Radiol* 1999; **9**: 555-562 [PMID: 10087133 DOI: 10.1007/s003300050709]
 - 9 **Menke J**, Unterberg-Buchwald C, Staab W, Sohns JM, Seif Amir Hosseini A, Schwarz A. Head-to-head comparison of prospectively triggered vs retrospectively gated coronary computed tomography angiography: Meta-analysis of diagnostic accuracy, image quality, and radiation dose. *Am Heart J* 2013; **165**: 154-163.e3 [PMID: 23351817 DOI: 10.1016/j.ahj.2012.10.026]
 - 10 **Sabarudin A**, Sun Z. Coronary CT angiography: Dose reduction strategies. *World J Cardiol* 2013; **5**: 465-472 [PMID: 24392191 DOI: 10.4330/wjc.v5.i12.465]
 - 11 **Sasdelli Neto R**, Nomura CH, Macedo AC, Bianco DP, Kay FU, Szarf G, Teles GB, Shoji H, Santana Netto PV, Passos RB, Chate RC, Ishikawa WY, Lima JP, Rocha MA, Marcos VN, Failla BB, Funari MB. Coronary computed tomography angiography with 320-row detector and using the AIDR-3D: initial experience. *Einstein (Sao Paulo)* 2013; **11**: 400-404 [PMID: 24136773 DOI: 10.1590/S1679-45082013000300025]
 - 12 **Xu L**, Zhang Z. Coronary CT angiography with low radiation dose. *Int J Cardiovasc Imaging* 2010; **26** Suppl 1: 17-25 [PMID: 20058080 DOI: 10.1007/s10554-009-9576-5]
 - 13 **Naoum C**, Blanke P, Leipsic J. Iterative reconstruction in cardiac CT. *J Cardiovasc Comput Tomogr* 2015; **9**: 255-263 [PMID: 26088375 DOI: 10.1016/j.jcct.2015.04.004]
 - 14 **Padole A**, Ali Khawaja RD, Kalra MK, Singh S. CT radiation dose and iterative reconstruction techniques. *AJR Am J Roentgenol* 2015; **204**: W384-W392 [PMID: 25794087 DOI: 10.2214/AJR.14.13241]
 - 15 **Shen H**, Dai G, Luo M, Duan C, Cai W, Liang D, Wang X, Zhu D, Li W, Qiu J. Image Quality and Radiation Dose of CT Coronary Angiography with Automatic Tube Current Modulation and Strong Adaptive Iterative Dose Reduction Three-Dimensional (AIDR3D). *PLoS One* 2015; **10**: e0142185 [PMID: 26599111 DOI: 10.1371/journal.pone.0142185]
 - 16 **Williams MC**, Weir NW, Mirsadraee S, Millar F, Baird A, Minns F, Uren NG, McKillop G, Bull RK, van Beek EJ, Reid JH, Newby DE. Iterative reconstruction and individualized automatic tube current selection reduce radiation dose while maintaining image quality in 320-multidetector computed tomography coronary angiography. *Clin Radiol* 2013; **68**: e570-e577 [PMID: 23838086 DOI: 10.1016/j.crad.2013.05.098]
 - 17 **Maurer MH**, Hamm B, Huppertz A, Lembcke A. Ultra-low-dose dual-source CT coronary angiography with high pitch: diagnostic yield of a volumetric planning scan and effects on dose reduction and imaging strategy. *Br J Radiol* 2015; **88**: 20140602 [PMID: 25710210 DOI: 10.1259/bjr.20140602]
 - 18 **Rybicki FJ**, Otero HJ, Steigner ML, Vorobiof G, Nallamshetty L, Mitsouras D, Ersoy H, Mather RT, Judy PF, Cai T, Coyner K, Schultz K, Whitmore AG, Di Carli MF. Initial evaluation of coronary images from 320-detector row computed tomography. *Int J Cardiovasc Imaging* 2008; **24**: 535-546 [PMID: 18368512 DOI: 10.1007/s10554-008-9308-2]
 - 19 **Chen MY**, Shanbhag SM, Arai AE. Submillisievert median radiation dose for coronary angiography with a second-generation 320-detector row CT scanner in 107 consecutive patients. *Radiology* 2013; **267**: 76-85 [PMID: 23340461 DOI: 10.1148/radiol.13122621]
 - 20 **Roberts WT**, Wright AR, Timmis JB, Timmis AD. Safety and efficacy of a rate control protocol for cardiac CT. *Br J Radiol* 2009; **82**: 267-271 [PMID: 19098083 DOI: 10.1259/bjr/24574758]
 - 21 **Dewey M**, Vavere AL, Arbab-Zadeh A, Miller JM, Sara L, Cox C, Gottlieb I, Yoshioka K, Paul N, Hoe J, de Roos A, Lardo AC, Lima JA, Clouse ME. Patient characteristics as predictors of image quality and diagnostic accuracy of MDCT compared with conventional coronary angiography for detecting coronary artery stenoses: CORE-64 Multicenter International Trial. *AJR Am J Roentgenol* 2010; **194**: 93-102 [PMID: 20028910 DOI: 10.2214/AJR.09.2833]
 - 22 **Stehli J**, Fuchs TA, Bull S, Clerc OF, Possner M, Buechel RR, Gaemperli O, Kaufmann PA. Accuracy of coronary CT angiography using a submillisievert fraction of radiation exposure: comparison with invasive coronary angiography. *J Am Coll Cardiol* 2014; **64**: 772-780 [PMID: 25145520 DOI: 10.1016/j.jacc.2014.04.079]
 - 23 **Moscariello A**, Takx RA, Schoepf UJ, Renker M, Zwerner PL, O'Brien TX, Allmendinger T, Vogt S, Schmidt B, Savino G, Fink C, Bonomo L, Henzler T. Coronary CT angiography: image quality, diagnostic accuracy, and potential for radiation dose reduction using a novel iterative image reconstruction technique-comparison with traditional filtered back projection. *Eur Radiol* 2011; **21**: 2130-2138 [PMID: 21611758 DOI: 10.1007/s00330-011-2164-9]
 - 24 **Alkadhi H**, Stolzmann P, Desbiolles L, Baumueller S, Goetti R, Plass A, Scheffel H, Feuchtner G, Falk V, Marincek B, Leschka S. Low-dose, 128-slice, dual-source CT coronary angiography: accuracy and radiation dose of the high-pitch and the step-and-shoot mode. *Heart* 2010; **96**: 933-938 [PMID: 20538669 DOI: 10.1136/hrt.2009.189100]
 - 25 **Litmanovich DE**, Tack DM, Shahrzad M, Bankier AA. Dose reduction in cardiothoracic CT: review of currently available methods. *Radiographics* 2014; **34**: 1469-1489 [PMID: 25310412 DOI: 10.1148/rg.346140084]
 - 26 **Achenbach S**, Marwan M, Ropers D, Schepis T, Pflederer T, Anders K, Kuettner A, Daniel WG, Uder M, Lell MM. Coronary computed tomography angiography with a consistent dose below 1 mSv using prospectively electrocardiogram-triggered high-pitch spiral acquisition. *Eur Heart J* 2010; **31**: 340-346 [PMID: 19897497 DOI: 10.1093/eurheartj/ehp470]
 - 27 **Hell MM**, Bittner D, Schubbaeck A, Muschiol G, Brand M, Lell M, Uder M, Achenbach S, Marwan M. Prospectively ECG-triggered high-pitch coronary angiography with third-generation dual-source CT at 70 kVp tube voltage: feasibility, image quality, radiation dose, and effect of iterative reconstruction. *J Cardiovasc Comput Tomogr* 2014; **8**: 418-425 [PMID: 25439789 DOI: 10.1016/j.jcct.2014.09.003]
 - 28 **Christner JA**, Kofler JM, McCollough CH. Estimating effective dose for CT using dose-length product compared with using organ doses: consequences of adopting International Commission on Radiological Protection publication 103 or dual-energy scanning. *AJR Am J Roentgenol* 2010; **194**: 881-889 [PMID: 20308486 DOI: 10.2214/AJR.09.3462]
 - 29 **Gosling O**, Loader R, Venables P, Roobottom C, Rowles N, Bellenger N, Morgan-Hughes G. A comparison of radiation doses between state-of-the-art multislice CT coronary angiography with iterative reconstruction, multislice CT coronary angiography with standard filtered back-projection and invasive diagnostic coronary angiography. *Heart* 2010; **96**: 922-926 [PMID: 20538667 DOI: 10.1136/hrt.2010.195909]

P- Reviewer: Bazeed MF, Pastromas S, Stavroulopoulos A
S- Editor: Wang JL **L- Editor:** A **E- Editor:** Tan WW





Published by **Baishideng Publishing Group Inc**
7901 Stoneridge Drive, Suite 501, Pleasanton, CA 94588, USA
Telephone: +1-925-223-8242
Fax: +1-925-223-8243
E-mail: bpgoffice@wjgnet.com
Help Desk: <http://www.f6publishing.com/helpdesk>
<http://www.wjgnet.com>

